

On the Optimal Integer-Forcing Precoding: A Geometric Perspective and a Polynomial-Time Algorithm

Junren Qin, Fan Jiang, Tao Yang, Shanxiang Lyu, Rongke Liu, *Senior Member, IEEE*, Shi Jin, *Fellow, IEEE*

Abstract

The joint optimization of the integer matrix \mathbf{A} and the power scaling matrix \mathbf{D} is central to achieving the capacity-approaching performance of Integer-Forcing (IF) precoding. This problem, however, is known to be NP-hard, presenting a fundamental computational bottleneck. In this paper, we reveal that the solution space of this problem admits a intrinsic geometric structure: it can be partitioned into a finite number of conical regions, each associated with a distinct full-rank integer matrix \mathbf{A} . Leveraging this decomposition, we transform the NP-hard problem into a search over these regions and propose the Multi-Cone Nested Stochastic Pattern Search (MCN-SPS) algorithm. Our main theoretical result is that MCN-SPS finds a near-optimal solution with a computational complexity of $\mathcal{O}(K^4 \log K \log_2(r_0))$, which is polynomial in the number of users K . Numerical simulations corroborate the theoretical analysis and demonstrate the algorithm's efficacy.

Index Terms

Overload MIMO, Integer-forcing precoding, Nonlinear optimization, Lattice basis reduction, Hybrid optimizer.

I. INTRODUCTION

Benefited from creating spatial diversity and performing spatial multiplexing, multiple-input multiple-output (MIMO) demonstrates powerful performance, and becomes the core technology of modern communication [1]. Developed through the massive MIMO (m-MIMO) [2] in fifth-generation (5G) and the Extremely large-scale MIMO (XL-MIMO) [3] in sixth-generation (6G), the reliability of communication is enhanced by the channel hardening effect [4] aroused when the number of antennas at base station (BS) N is larger than the number of single antenna

This work was supported in part by Mobile Information Networks National Science and Technology Major Project under Grant No.2025ZD1305200, in part by Low-Altitude Airspace Strategic Program Portfolio under Grant Z25306105.

Junren Qin is with the School of Electronics Information Engineering, Beihang University, Beijing 100191, China, the Pengcheng Laboratory (PCL), Shenzhen 518066, China, and the Shenzhen Institute of Beihang University, Shenzhen, China (e-mail: junrenqin@buaa.edu.cn).

Fan Jiang is with the Pengcheng Laboratory (PCL), Shenzhen 518066, China (e-mail: jiangf02@pcl.ac.cn).

Shanxiang Lyu is with the College of Cyber Security, Jinan University, Guangzhou 510632, China (E-mail: lxx07@jnu.edu.cn).

Tao Yang are with the School of Electronics Information Engineering, Beihang University, Beijing 100191, China (e-mail: tyang@buaa.edu.cn).

Rongke Liu is with the Shenzhen Institute of Beihang University, Shenzhen, China, and is also with the School of Electronics Information Engineering, Beihang University, Beijing 100191, China (e-mail: rongke_liu@buaa.edu.cn).

Shi Jin is with the School of Information Science and Engineering, Southeast University, Nanjing 210096, China (e-mail: jinshi@seu.edu.cn).

Corresponding author: Rongke Liu, Tao Yang, Fan Jiang.

user equipments (UEs) K . Towards the massive communication and ubiquitous connectivity applications in 6G, the demand for increased connectivity and user density has become a key performance indicator, and the increasing trend of these parameters is expected to continue in near future [5]. This trend rise an attention on the overload MIMO system, in which $K \geq N$ and the occurrence of channel hardening effects is impeded by the limited spatial freedom.

Considering the downlink, the messages are delivered from BS to UEs, which enables all messages of UEs to broadcast with full bandwidth. The capacity region of MIMO broadcasting (BC) channel can be established from the capacity region of MIMO multiple-access channel via the uplink-downlink duality, and can be achieved so far by dirty-paper coding (DPC) [6], [7]. Unfortunately, since the high implementation complexity, DPC is widely regarded as a theoretical tool. To decrease the complexity under a tradeoff on performance, Tomlinson-Harashima Precoding (THP) [8] employs the decision feedback equalization (DFE) into the transmitter side. Furthermore, vector-perturbation (VP) [9], [10] precoding regards the interference cancellation process of DFE as the solution of closest vector problem (CVP) in lattice theory [11]. To minimize transmission power, VP employs an accurate sphere decoder (SD) combined Lenstra-Lenstra-Lovász (LLL) algorithm [12] and sphere decoding algorithm [13]. These methods are all realized under the inspiration of interference canceling, which cannot be directly applied to the overload MIMO. As a large-scale UEs are distributed into less BS in the channel, the multi-user inference (MUI) is unable to eliminate completely, making it defective to the idea of interference canceling. Meanwhile, the lack of spatial dimension in the overload MIMO decrease the accuracy of successive interference cancellation (SIC) in THP, and lose the effectiveness of LLL algorithm in VP. These lead to a weak performance on THP and a high complexity on VP.

On the other hand, the linear precoding rectify MUI by multiplying a precoding matrix related to channel matrix with the signal or message, and becoming a large class due to its easy-to-implement characteristics. The popular methods in this category are zero-forcing (ZF) precoding and regularized ZF (RZF) precoding [14]–[16]. For the precoding matrix, ZF employs the inverse (or pseudo inverse) of channel matrix, and RZF conducted a normalization matrix by minimum mean square error (MMSE) filtering. When $N \gg K$ in MMIMO or XL-MIMO, both ZF and RZF can approach the channel capacity [1], [17], but the situation is quite the opposite in the overload MIMO. Regarding the ZF, since the channel matrix is full column-rank, the multiplication between channel matrix and its pseudo inverse outputs the least norm and least square solution, and the gap between the outputs and identity matrix are enlarged during the ratio K/N expansion. Meanwhile, in the pseudo inverse of channel matrix, the expansion of condition number under the overload MIMO cause the increased additive noise contained in the outputs of precoder. Although these flaws are attenuated in RZF by the MMSE filter, the effects caused by overload MIMO are still non-negligible and an adaptable solution for overload MIMO is required.

Recently, based on the lattice-reduction-aided (LRA) precoding [18] and compute-and-forward (CF) [19], the integer-forcing (IF) precoding [20] provides a effective methods to restrain MUI without a significant increased complexity. Rather than separating users' codeword by the equalization and beamforming, IF precoder applies inverse linear transforming to correspond the integer-linear combination (ILC) to the desired message of that user [20]. As this reason, IF precoder can universally achieve the MIMO capacity to within a constant gap [21]. Regarding

the overload MIMO, the ILC provides a degree of freedom to offset the effects caused by the dimensional flaw, which make IF precoding exhibiting a good adaptability to overloaded MIMO. In the IF precoding, the performance relates to the selection of a proper linear precoding matrix \mathbf{P} . To achieve this optimization for general signal-to-noise ratio (SNR), [20] shows that the optimal selection of \mathbf{P} is to choose a proper (unimodular) integer-valued matrix \mathbf{A} and the beamforming matrix \mathbf{D} such that $\mathbf{HP} \approx c\mathbf{DA}$, and becomes equivalent when $\text{SNR} \rightarrow \infty$. As a results, the research on IF precoder designing mainly focuses on the joint optimization between \mathbf{A} and \mathbf{D} . For the special case that $K = 2$, Silva *et. al* [20] provide the optimal pair (\mathbf{A}, \mathbf{D}) . in high SNR. In general case, He *et. al* [22] propose an iterative algorithm based on uplink-downlink duality to calculate the optimal (\mathbf{A}, \mathbf{D}) accurately. Qiu *et. al* [23] obtain the optimal (\mathbf{A}, \mathbf{D}) via the Particle Swarm Optimization (PSO) algorithm [24]. Considering the requirements of low-complexity and sub-optimal optimization in general case, Venturelli *et. al* [25] propose an calculation-constraint-relaxed algorithm form integer-valued full-rank matrix \mathbf{A} to complex-valued upper-unitriangular matrix \mathbf{A} .

Nevertheless, the aforementioned methods face three critical tradeoffs:

- **Optimality vs. Feasibility:** Iterative algorithms based on uplink-downlink duality may yield power allocations incompatible with practical constraints like a common shaping lattice [22].
- **Global vs. Local Search:** Heuristic methods like Particle Swarm Optimization (PSO) are prone to getting trapped in local optima and incur high computational costs [23], [26].
- **Accuracy vs. Complexity:** Relaxation-based methods simplify the problem by constraining \mathbf{A} to a relaxed form (e.g., complex upper-unitriangular), but this often leads to performance loss [25].

Thus, designing an algorithm that efficiently navigates this joint optimization to strike a superior complexity-accuracy trade-off remains an open and significant challenge.

The contributions of this article, along with the highlights, are summarized as follows.

- **Geometric Problem Reformulation:** We establish a generalized optimization model that reveals the underlying geometric structure of the solution space. By treating \mathbf{A} as a function of \mathbf{D} , we map the problem to a search within a $(K - 1)$ -dimensional space Ω . We prove that Ω can be partitioned into a finite number of conical regions, each corresponding to a distinct, fixed integer matrix \mathbf{A} . A key insight is that any point within such a region can be uniquely represented by the direction of a ray from the origin, which drastically simplifies the subsequent search. This decomposition transforms the continuous joint optimization into a structured search over discrete regions.
- **Polynomial-Time Algorithm Design:** MCN-SPS adopts a stochastic, nested search strategy that iteratively explores candidate conical regions. At each iteration, it constructs a hypersphere centered at the current point and generates multiple sampling points via randomly directed rays. Each sampling point is projected back to the constraint set Ω and then fed into an efficient alternating optimization (AO) subroutine to obtain a local optimum. By comparing the sum rates of these local optima with the current point, MCN-SPS either shifts its search center to a better solution or contracts the search radius, thereby systematically refining its exploration. Crucially, within the AO subroutine, we develop a direction-guided method for \mathbf{D} -optimization that employs

a contraction mapping in the Hilbert metric space, ensuring fast convergence. By discretizing the continuous search space into these structured regions and leveraging efficient local optimization, MCN-SPS achieves both low time complexity and high accuracy in solving the (\mathbf{A}, \mathbf{D}) optimization problem.

- **Theoretical and Numerical Validation:** We rigorously analyze the computational complexity of MCN-SPS, proving it to be $\mathcal{O}(K^4 \log K \log_2(r_0))$ with LLL algorithm, which is polynomial in K . Extensive simulations corroborate this analysis, demonstrating that MCN-SPS achieves a lower computational cost than the PSO-based benchmark. Moreover, it delivers superior sum-rate performance, outperforming all compared methods, especially in overloaded MIMO scenarios.

Notation: Matrices and column vectors are denoted by uppercase and lowercase boldface letters. Specially, for a matrix \mathbf{X} , we denote its i -th column vector as \mathbf{x}_i , and represents the i -th row vector as \mathbf{x}_i^\top . We represent the set by uppercase squiggles letters. For any $x > 0$, let $\log^+(x) \triangleq \max\{0, \log(x)\}$. Considering the multiplying for matrix \mathbf{A} and \mathbf{B} , we denote the dot product as $\mathbf{A}\mathbf{B}$, and the Hadamard product as $\mathbf{A} \circ \mathbf{B}$. Regarding two vector \mathbf{x} and \mathbf{y} , we define $\mathbf{x} \oslash \mathbf{y}$ the element-wise division which outputs a vector $[x_1/y_1, \dots, x_n/y_n]^\top$. Considering multiplication in symbol calculation, the term \otimes is represented as modulo- p multiplication. The operation $\text{diag}(\cdot)$ represents obtaining a vector contained the main diagonal elements of the inputted matrix.

II. PRELIMINARIES

A. System Model

Regarding a single-cell system consisting of a BS with N antenna and K single-antenna UEs, the BS broadcasts signals to the UEs, and each UE acquires their correspond message in the received signal from BS. In each broadcasting, considering $k \in \{1, \dots, K\}$, $n \in \{1, \dots, N\}$, the coded-modulated signal matrix $\mathbf{X} = [\mathbf{x}_1, \dots, \mathbf{x}_N]$, where $\mathbf{x}_n = [x_{1,n}, \dots, x_{K,n}]^\top$, is modeled by the signal-level matrix \mathbf{P} with the power constraint

$$\text{Tr}(\mathbf{P}\mathbf{P}^\top) \leq \rho, \quad (1)$$

where ρ represents the transmit power at BS. Each precoded signals $\mathbf{s}[n]$ from the N antennas of BS is given by

$$\mathbf{s}[n] = \mathbf{P}[n]\mathbf{x}[n], \quad (2)$$

where $\mathbf{x}[n] = \mathbf{x}_n = [x_{1,n}, \dots, x_{K,n}]^\top$ denotes the K signals at the t -th instant (or sub-carrier) of the block.

Regarding the transmission in channel, each $\mathbf{s}[n]$ is affected by channel coefficient vector $\mathbf{h}_i^\top[n]$ and the additive white Gaussian noise (AWGN) $z_i[n]$ with zero mean and unit variance $\sigma_z^2 = 1$, where i represents the index of UE. For a real-valued model, the base-band equivalent received signal of the i -th UE $y_i[n]$ is calculated by

$$y_i[n] = \mathbf{h}_i^\top[n]\mathbf{s}[n] + z_i[n]. \quad (3)$$

Considering the channel coefficient matrix $\mathbf{H}^{K \times N}[n] = [\mathbf{h}_1^\top[n], \dots, \mathbf{h}_K^\top[n]]^\top$, the received signals of the K UEs are

$$\mathbf{y}[n] = \mathbf{H}[n]\mathbf{s}[n] + \mathbf{z}[n], \quad (4)$$

where $\mathbf{z}[n]$ denotes the AWGN vector. The transmission signal-to-noise ratio (SNR) is given by ρ . In this paper, we present a real-valued model, and the complex-valued model with $\check{\mathbf{H}} \in \mathbb{C}$ can be represented by a real-valued model of doubled dimension, i.e.,

$$\begin{bmatrix} \Re\{\mathbf{Y}\} \\ \Im\{\mathbf{Y}\} \end{bmatrix} = \begin{bmatrix} \Re\{\check{\mathbf{H}}\} & -\Im\{\check{\mathbf{H}}\} \\ \Im\{\check{\mathbf{H}}\} & \Re\{\check{\mathbf{H}}\} \end{bmatrix} \begin{bmatrix} \Re\{\mathbf{s}\} \\ \Im\{\mathbf{s}\} \end{bmatrix} + \begin{bmatrix} \Re\{\mathbf{z}\} \\ \Im\{\mathbf{z}\} \end{bmatrix}, \quad (5)$$

as treated in [19], [20].

In practice, the channel matrix \mathbf{H} has to be estimated at the receiver for retrieving the transmitted data symbol vector, and imperfect channel estimates arise in any practical estimation scheme [27]. In this paper, we consider the conventional channel estimations on minimum mean-square error (MMSE) [28] and maximum likelihood (ML) [29]. In the MMSE channel estimation, the channel state information (CSI) with channel estimation error is modeled as [28]

$$\mathbf{H} = \hat{\mathbf{H}} + \mathbf{E}, \quad (6)$$

where $\hat{\mathbf{H}}$ and $\mathbf{E} \sim \mathcal{N}(0, \sigma_e^2 \mathbf{I})$ denote the estimated channel and its estimation error respectively. Under the principle of minimum observation-error distance, $\hat{\mathbf{H}}$ is independent to \mathbf{E} . Regarding ML channel estimation, the channel estimate can be given as [29]

$$\hat{\mathbf{H}} = \mathbf{H} + \mathbf{E}, \quad (7)$$

where the practical channel $\mathbf{H} \sim \mathcal{N}(0, \sigma_h^2) \mathbf{I}$ is independent to $\mathbf{E} \sim \mathcal{N}(0, \sigma_e^2) \mathbf{I}$. In ML case, σ_e^2 can be calculated by [27]

$$\sigma_e^2 = \frac{K \sigma_z^2}{N_{\text{train}} E_{\text{train}}}, \quad (8)$$

where N_{train} and E_{train} respectively denote the length of the training sequence and the power of the training symbols.

B. Integer-Forcing (IF) Precoding

Differ to the conventional linear precoding, IF precoding employs the users' codeword to create an integer-valued effective channel matrix. By applying inverse linear transforming to correspond the ILC to the desired message of that user, IF precoder can universally achieve the MIMO capacity to within a constant gap [20], [21]. According to [22], [23], the flowchart of IF precoding system is depicted in Fig. 1. The whole procedure consists of the transmitter, receivers, and joint optimization.

1) *Transmitter*: Before transmitting, a full rank integer-valued matrix $\mathbf{A} \in \mathbb{Z}^{K \times K}$ and a positive diagonal matrix $\mathbf{D} = \text{diag}(d_1, \dots, d_K)$ are selected by the joint optimization. Moreover, \mathbf{D} satisfies

$$\det(\mathbf{D}) = 1. \quad (9)$$

In BS, K modulo- p UE-corresponded messages $\mathbf{c}_1, \mathbf{c}_2, \dots, \mathbf{c}_K \in \mathbb{Z}_p$ are modified by multiplying a matrix \mathbf{Q}^{-1} satisfied $\mathbf{Q}^{-1} \otimes \mathbf{Q} = \mathbf{I}$, where

$$\mathbf{Q} \equiv \lfloor \mathbf{A} \rfloor \pmod{p} \quad (10)$$

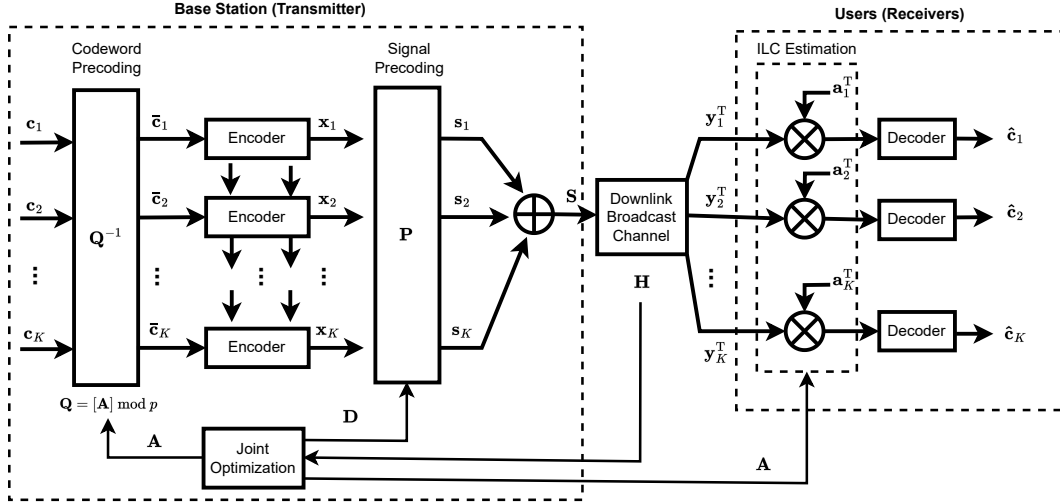


Fig. 1. Block diagram of the IF precoding architecture [22], [23]

over \mathbb{Z}_p . The outputs $\bar{\mathbf{c}}_k = \mathbf{Q}^{-1} \otimes \mathbf{c}_k$, $k \in \{1, \dots, K\}$, are mapped into K *codeword-level precoded (CLP) p-PAM* symbols $\mathbf{x}_1, \dots, \mathbf{x}_K$ by

$$\mathbf{x}_k = \frac{1}{\gamma} \left(\bar{\mathbf{c}}_k - \frac{p-1}{2} [1, \dots, 1]^\top \right) \in \frac{1}{\gamma} \left\{ \frac{1-p}{2}, \dots, \frac{p-1}{2} \right\}^K. \quad (11)$$

Then, a precoder \mathbf{P} handles these CLP streams to the *Signal-level precoded (SLP)* streams $\mathbf{s}_1, \dots, \mathbf{s}_K$ by Eq. (2), which are then transmitted via the N antennas of BS. According to [20], similar to ZF and RZF, \mathbf{P} can be obtained by

$$\mathbf{P} = \frac{1}{\eta} \mathbf{H}^\top (\mathbf{H}\mathbf{H}^\top)^{-1} \mathbf{D}\mathbf{A} \quad (12)$$

for diagonally-scaled exact IF (DIF), and

$$\mathbf{P} = \frac{1}{\eta} \mathbf{H}^\top \left(\frac{K}{\rho} \mathbf{I} + \mathbf{H}\mathbf{H}^\top \right)^{-1} \mathbf{D}\mathbf{A} \quad (13)$$

for regularized IF (RIF). In Eq. (12) and Eq. (13), each entry d_k , $k \in \{1, \dots, K\}$ denotes the power allocated to the k -th CLP stream, and η is a scalar to ensure that the power constraint Eq. (1) is met. Regarding the full column rank channel matrix \mathbf{H} in overload MIMO, RIF is suitable since $\mathbf{H}\mathbf{H}^\top$ is not a full-rank matrix but $\frac{K}{\rho} \mathbf{I} + \mathbf{H}\mathbf{H}^\top$ is.

2) *Receivers*: According to Eq. (11), the received signal of UE k in Eq. (3) can be written as

$$y_k = \mathbf{h}_k^\top \mathbf{s}_k + z_k = \mathbf{h}_k^\top \mathbf{P} \mathbf{x}_k + z_k = \frac{1}{\gamma} \tilde{\mathbf{h}}_k^\top \bar{\mathbf{c}}_k + z_k - \underbrace{\frac{p-1}{2\gamma} \sum_{l=1}^K \tilde{h}_{k,l}}_{\text{not related to the signal}}, \quad (14)$$

where $\tilde{\mathbf{h}}_k^\top = \mathbf{h}_k^\top \mathbf{P} = [\tilde{h}_{k,1}, \dots, \tilde{h}_{k,N}]$. Since $\bar{\mathbf{c}}_k$ is an integer-valued vector, $\tilde{\mathbf{h}}_k^\top \bar{\mathbf{c}}_k$ can be regarded as the k -th entry of lattice point with basis $[\tilde{\mathbf{h}}_1^\top, \dots, \tilde{\mathbf{h}}_K^\top]^\top$, and y_k as a dithering on the i -th lattice point which can be compensated easily.

At the receivers, receiver k computes the ILC of $\bar{\mathbf{c}}_k$, written as

$$\hat{\mathbf{s}}_{k,n} = \mathbf{a}_k^\top \otimes \bar{\mathbf{c}}_k, \quad k \in \{1, \dots, K\}, \quad n \in \{1, \dots, N\}, \quad (15)$$

based on the noisy observation of the lattice points in Eq. (14). According to Eq. (10), Eq. (15) can be rewritten as

$$\hat{\mathbf{s}}_{k,n} = \mathbf{a}_k^\top \otimes \bar{\mathbf{c}}_k = \mathbf{a}_k^\top \otimes \mathbf{A}^{-1} \otimes \mathbf{c}_k = \hat{\mathbf{c}}_k. \quad (16)$$

Then, the computed stream of UE- k $\hat{\mathbf{s}}_k$ is shifted into the estimated message $\hat{\mathbf{c}}_1, \dots, \hat{\mathbf{c}}_K$.

3) *Joint Optimization*: The achievable rate of IF precoding can be obtained simply by

$$R_i(\mathbf{A}) \triangleq \log_2^+ \left(\frac{1}{\mathbf{a}_i \left(\mathbf{I} - \frac{\rho}{\rho \|\tilde{\mathbf{h}}_i\|^2 + 1} \tilde{\mathbf{h}}_i^\top \tilde{\mathbf{h}}_i \right) \mathbf{a}_i^\top} \right), \quad (17)$$

where $\tilde{\mathbf{h}}_i^\top = \mathbf{h}_i^\top \mathbf{P}$ and we use the function $\log^+(x) = \max(x, 0)$ to ensure that the rate remains non-negative.

For the high SNR regime [23], IF precoding is optimal and can achieve a sum rate given by

$$R(\mathbf{A}, \mathbf{D}) = \frac{1}{2} \sum_{i=1}^K \log_2^+ \left(\frac{d_i^2 \rho}{\text{Tr}(\mathbf{A}^\top \mathbf{D}^\top \mathbf{M} \mathbf{D} \mathbf{A})} \right) = \frac{K}{2} \log_2^+ \left(\frac{\rho (\det(\mathbf{D}))^2}{\text{Tr}(\mathbf{A}^\top \mathbf{D}^\top \mathbf{M} \mathbf{D} \mathbf{A})} \right), \quad (18)$$

where

$$\mathbf{M} = (\mathbf{H} \mathbf{H}^\top)^{-1} \quad (19)$$

in DIF precoding, and

$$\mathbf{M} = \left(\frac{K}{\rho} \mathbf{I} + \mathbf{H} \mathbf{H}^\top \right)^{-1} \quad (20)$$

in RIF precoding. The target of (\mathbf{A}, \mathbf{D}) joint optimization is to select a pair of (\mathbf{A}, \mathbf{D}) to maximize Eq. (18). Under the constraint in Eq. (9) and the Monotonic property of $\log(\cdot)$ function, this problem can be expressed to

$$\arg \min_{\mathbf{A}, \mathbf{D}} \quad \text{Tr}(\mathbf{A}^\top \mathbf{D}^\top \mathbf{M} \mathbf{D} \mathbf{A}), \quad (21)$$

$$\text{subject to} \quad \mathbf{A} \in \mathbb{Z}^{K \times K}, \quad \text{rank}(\mathbf{A}) = K, \quad \mathbf{D} \in \mathbb{R}_+^{K \times N}, \quad |\det(\mathbf{D})| = 1.$$

Considering a fixed \mathbf{D} , the optimization of \mathbf{A} is equivalent to minimize

$$\text{Tr}(\mathbf{A}^\top \mathbf{D}^\top \mathbf{M} \mathbf{D} \mathbf{A}) = \sum_{l=1}^K \|\mathbf{M}^{\frac{1}{2}} \mathbf{D} \mathbf{a}_l\|^2, \quad (22)$$

where \mathbf{a}_l denotes the l -th column of \mathbf{A} . Regarding $\mathbf{M}^{\frac{1}{2}} \mathbf{D}$ as a lattice basis, to minimize Eq. (22) is to solve the well-known shortest independent vector problem (SIVP) [30] in lattice theory.

C. Lattice Basis Reduction

This paper will use some concepts from lattices to arrive at simpler description of the algorithm and more elegant analysis. Hereby we review some basic concepts of lattices and lattice reduction. An M -dimensional lattice in \mathbb{R}^M is defined as

$$\Lambda = \{ \mathbf{G} \mathbf{z} | \mathbf{z} \in \mathbb{Z}^M \}, \quad (23)$$

where the full-ranked matrix $\mathbf{G} \in \mathbb{R}^{M \times M}$ represents the generator matrix of Λ . In a lattice Λ , SIVP is one of the critical problem to describe the structure of lattice, which is defined in Definition 1.

Definition 1 (SIVP [12]). *Given a lattice $\Lambda \in \mathbb{R}^M$, find M linearly independent vectors $\mathbf{v}_1, \dots, \mathbf{v}_M \in \Lambda$, such that*

$$\|\mathbf{v}_m\| \leq \lambda_M(\Lambda), \quad m \in \{1, \dots, M\} \quad (24)$$

In Definition 1, $\lambda_M(\Lambda)$ represents the M -th successive minima which is given by Definition 2.

Definition 2 (Successive Minima [12]). *Considering a lattice $\Lambda \in \mathbb{R}^M$ and $\forall i \in \{1, \dots, \dim(\Lambda)\}$, the i -th minimum $\lambda_i(\Lambda)$ is defined as the minimum of $\max_{1 \leq j \leq i} \|\mathbf{v}_j\|$ over all i linearly independent lattice vector $\mathbf{v}_1, \dots, \mathbf{v}_i \in \Lambda$*

To solve SIVP, many existing methods [13], [31]–[33] have been proposed. In this paper, we focus on the conventional LLL algorithm [31] due to its polynomial complexity. The corresponded metric of LLL algorithm, referred to as LLL reduced basis, is defined in Definition 3.

Definition 3 (LLL reduced [32]). *Let \mathbf{R} be the R matrix of a QR decomposition on \mathbf{G} , with elements $r_{i,j}$'s. A basis \mathbf{G} is called LLL reduced if the following two conditions hold:*

- i) $|r_{i,j}/r_{i,i}| \leq \frac{1}{2}$, $1 \leq i < j \leq N$. (Size Reduction conditions)
- ii) $\delta \|\pi_{\mathbf{G}}^\perp(\mathbf{g}_i)\|^2 \leq \|\pi_{\mathbf{G}}^\perp(\mathbf{g}_{i+1})\|^2$, $1 \leq i \leq N - 1$. (Lovász conditions)

In Definition 3, $\delta \in (\frac{1}{4}, 1]$ is called the Lovász constant, and an equivalently rewritten form of Lovász conditions is

$$\|\mathbf{g}_{i+1}^*\|^2 \leq (\delta - \mu_{i+1}^2) \|\mathbf{g}_i^*\|^2. \quad (25)$$

If \mathbf{G} is LLL reduced, it satisfies [31]

$$\|\mathbf{g}_i\| \leq \beta^{N-1} \lambda_i(\Lambda_{\mathbf{G}}), \quad i \in \{1, \dots, N\}, \quad (26)$$

in which

$$\beta = \frac{1}{\sqrt{\delta - \frac{1}{4}}} \in \left(\frac{2}{\sqrt{3}}, +\infty \right). \quad (27)$$

In the LLL algorithm, summarized in Alg. 1, the operation i and ii can be regarded as two transforming matrix $\mathbf{T}_{k,i}^{(i)}$ and $\mathbf{T}_i^{(ii)}$ respectively satisfy

$$\mathbf{T}_{k,i}^{(i)} = \begin{bmatrix} 1 & -\mu_{k,i} \\ 0 & 1 \end{bmatrix}, \quad \mathbf{T}_i^{(ii)} = \begin{bmatrix} 0 & 1 \\ 1 & 0 \end{bmatrix}, \quad (28)$$

where $\mathbf{T}_{k,i}^{(i)}$ is implemented on a pair of vector $[\mathbf{r}_k, \mathbf{r}_i]$ and $\mathbf{T}_i^{(ii)}$ on $[\mathbf{r}_{i-1}, \mathbf{r}_i]$. In the LLL algorithm processing, the transforming matrix between the original and LLL reduced basis is a unimodular matrix which is derived by multiplying all $\mathbf{T}_{k,i}^{(i)}$ and $\mathbf{T}_i^{(ii)}$ continuously under their order in the process [34].

D. The Contraction Mapping Approach to Perron-Frobenius Theory

In this paper, we employ the Perron-Frobenius Theory in the complete metric space of Hilbert metric to guide the algorithm design. Hereby, we review some knowledge about the contraction mapping approach [35]–[37] and nonlinear Perron-Frobenius theory [38].

Algorithm 1 The LLL algorithm**Input:** Lattice basis matrix \mathbf{G} , Lovász constant δ **Output:** LLL-reduced basis matrix \mathbf{G}' , Transforming unimodular matrix \mathbf{A}

```

1:  $[\mathbf{Q}, \mathbf{R}] \leftarrow \text{qr}(\mathbf{G})$  ▷ The QR Decomposition of  $\mathbf{G}$ 
2:  $[M, N] \leftarrow \text{size}(\mathbf{G})$ 
3:  $i \leftarrow 2$ 
4: while  $i \leq N$  do
5:   for  $k = i - 1 : -1 : 1$  do
6:      $\mu_{k,i} = \lfloor r_{k,i}/r_{i,i} \rfloor$  ▷  $r_{i,j}$  is the  $(i, j)$  element of  $\mathbf{R}$ 
7:     if  $\mu \neq 0$  then ▷ Operation i
8:        $\mathbf{r}_i \leftarrow \mathbf{r}_i - \mu_{k,i} \mathbf{r}_k$  ▷  $\mathbf{r}_i$  is the  $i$ -th column of  $\mathbf{R}$ 
9:     end if
10:  end for
11:  if  $\delta |r_{i-1,i-1}|^2 > |r_{i,i}|^2 + |r_{i-1,i}|^2$  then
12:     $\alpha = r_{i-1,i} / \sqrt{r_{i-1,i}^2 + r_{i,i}^2}$ 
13:     $\beta = r_{i,i} / \sqrt{r_{i-1,i}^2 + r_{i,i}^2}$ 
14:    Swap  $\mathbf{r}_{i-1}$  and  $\mathbf{r}_i$  ▷ Operation ii
15:     $\mathbf{V} \leftarrow \begin{bmatrix} \alpha & \beta \\ -\beta & \alpha \end{bmatrix}$ 
16:     $\begin{bmatrix} \mathbf{r}_{i-1}^\top \\ \mathbf{r}_i^\top \end{bmatrix} \leftarrow \mathbf{V} \begin{bmatrix} \mathbf{r}_{i-1}^\top \\ \mathbf{r}_i^\top \end{bmatrix}$  ▷  $\mathbf{r}_i^\top$  is the  $i$ -th row of  $\mathbf{R}$ 
17:     $[\mathbf{q}_{i-1}, \mathbf{q}_i] \leftarrow [\mathbf{q}_{i-1}, \mathbf{q}_i] \mathbf{V}^\top$  ▷  $\mathbf{q}_i$  is the  $i$ -th column of  $\mathbf{Q}$ 
18:     $i \leftarrow \max(i - 1, 2)$ 
19:  else
20:     $i \leftarrow i + 1$ 
21:  end if
22: end while
23:  $\mathbf{G}' \leftarrow \mathbf{QR}$ 
24:  $\mathbf{A} \leftarrow \lfloor \mathbf{G}^{-1} \mathbf{G}' \rfloor$  ▷  $\lfloor \cdot \rfloor$  round for all elements

```

In a complete metric space (\mathcal{X}, d) , a linear transformation \mathbf{T} is a contraction when it satisfy

$$\exists \gamma \in (0, 1), d(\mathbf{T}\mathbf{x}, \mathbf{T}\mathbf{y}) \leq \gamma d(\mathbf{x}, \mathbf{y}), \forall \mathbf{x}, \mathbf{y} \in \mathcal{X}. \quad (29)$$

For a contraction \mathbf{T} , there exists an $\mathbf{x}_0 \in \mathcal{X}$ such that $\mathbf{T}^q \mathbf{x} \mapsto \mathbf{x}_0$ for all $\mathbf{x} \in \mathcal{X}$, where \mathbf{x}_0 is referred to as the fixed point for \mathbf{T} in (\mathcal{X}, d) . In direction, the well-known Perron Theorem [36] tells that if \mathbf{T} is a positive linear transformation on \mathbb{R}^N , then it has

$$\exists \mathbf{x}_0, \mathbf{x} > 0, \text{ such that (s.t.), } \frac{\mathbf{T}\mathbf{x}}{\|\mathbf{T}\mathbf{x}\|} \rightarrow \frac{\mathbf{x}_0}{\|\mathbf{x}_0\|}. \quad (30)$$

In [35], [39], a Hilbert metric $d_H(\cdot)$ in non-Euclidean geometry is defined as

$$d_H(\mathbf{x}, \mathbf{y}) = \log \left(\frac{\max(\mathbf{x} \oslash \mathbf{y})}{\min(\mathbf{x} \oslash \mathbf{y})} \right). \quad (31)$$

And it has the following characteristics [37]:

- i) $d_H(\mathbf{x}, \mathbf{y}) \geq 0$, and $d_H(\mathbf{x}, \mathbf{y}) = 0$ if and only if $\mathbf{x} = c\mathbf{y}$, $c > 0$.
- ii) $d_H(\mathbf{x}, \mathbf{y}) = d_H(\mathbf{y}, \mathbf{x})$.
- iii) $d_H(\mathbf{x}, \mathbf{z}) \leq d_H(\mathbf{x}, \mathbf{y}) d_H(\mathbf{y}, \mathbf{z})$.
- iv) $d_H(\mathbf{x}, \mathbf{z}) \leq d_H(\mathbf{x}, \mathbf{y}) + d_H(\mathbf{y}, \mathbf{z})$.
- v) $\forall a, b > 0$, $d_H(a\mathbf{x}, b\mathbf{y}) = d_H(\mathbf{x}, \mathbf{y})$.

Regarding the Hilbert metric, the Perron Theorem still works, referring to as the Birkhoff-Hopf theorem, denoted by

$$d_H(\mathbf{T}\mathbf{x}, \mathbf{T}\mathbf{y}) \leq \gamma d_H(\mathbf{x}, \mathbf{y}), \forall \mathbf{x}, \mathbf{y} \in \mathcal{X}, \quad (32)$$

where $\exists \gamma \in (0, 1)$, and \mathbf{T} is non-positive. The contraction ratio $\kappa(\mathbf{T})$ of a linear operator \mathbf{T} is defined in [38] as

$$\kappa(\mathbf{T}) \triangleq \inf \{ \gamma \geq 0 \mid d_H(\mathbf{T}\mathbf{x}, \mathbf{T}\mathbf{y}) \leq \gamma d_H(\mathbf{x}, \mathbf{y}), \forall \mathbf{x}, \mathbf{y} \in \mathcal{X} \}. \quad (33)$$

In [35], it is proved that

$$\kappa(\mathbf{T}) = \tanh \left(\frac{\Delta(\mathbf{T})}{4} \right), \quad (34)$$

where the projective diameter $\Delta(\mathbf{T})$ of \mathbf{T} is defined by

$$\Delta(\mathbf{T}) \triangleq \sup \{ d_H(\mathbf{T}\mathbf{x}, \mathbf{T}\mathbf{y}) \mid \mathbf{x}, \mathbf{y} \in \mathcal{X} \}. \quad (35)$$

III. GEOMETRIC STRUCTURE OF THE SOLUTION SPACE

Since $\mathbf{D} = \text{diag}(d_1, \dots, d_K)$ is a positive diagonal matrix with $\det(\mathbf{D}) = 1$, the set of all possible \mathbf{D} is the positive diagonal subgroup of special linear group $\text{SLD}_K^+(\mathbb{R})$. To express \mathbf{D} in simple, we define its main diagonal as a vector \mathbf{d} by

$$\mathbf{d} = [d_1, \dots, d_K]^\top, \quad (36)$$

where $\mathbf{1}_K = [1, \dots, 1]^\top$. Since the elements $\{d_k\}_{k=1}^K$ are all positive, following the constraint in Eq. (9), \mathbf{d} satisfies $\prod_{k=1}^K d_k = 1$, or $\sum_{k=1}^K \log(d_k) = 0$. Regarding $\{d_k\}_{k=1}^K$ as the positive region coordinates of a K dimensional space \mathcal{D} , the set of all possible \mathbf{d} for Eq. (21) is a $K - 1$ dimensional subspace Ω represented by

$$\Omega = \left\{ \mathbf{d} \mid \prod_{k=1}^K d_k = 1, d_k > 0, k \in 1, \dots, K \right\}. \quad (37)$$

In this section, we will elaborate a generalized optimization model for IF precoding with the geometric features of \mathcal{D} .

A. General Model of Joint Optimization

According to Eq. (22), we can regard \mathbf{A} as a function related to \mathbf{d} , referring to as $\mathbf{A}(\mathbf{d})$. To correspond \mathcal{D} , the expression in Eq. (21) can be rewritten as

$$\text{Tr}(\mathbf{A}(\mathbf{d})^\top \mathbf{D}^\top \mathbf{M} \mathbf{D} \mathbf{A}(\mathbf{d})) = \mathbf{d}^\top ((\mathbf{A}(\mathbf{d}) \mathbf{A}(\mathbf{d})^\top) \circ \mathbf{M}) \mathbf{d}. \quad (38)$$

Thus, the problem in (21) is equivalent to

$$\begin{aligned} \arg \min_{\mathbf{d}} \quad & \mathbf{d}^\top ((\mathbf{A}(\mathbf{d}) \mathbf{A}(\mathbf{d})^\top) \circ \mathbf{M}) \mathbf{d}, \\ \text{subject to} \quad & \mathbf{d} \in \Omega. \end{aligned} \quad (39)$$

Considering the interference coupling matrix $\mathbf{G} = (\mathbf{A} \mathbf{A}^\top) \circ \mathbf{M}$, since \mathbf{M} is known, \mathbf{G} is also a function related to \mathbf{d} , denoted as $\mathbf{G}(\mathbf{d})$. The Lagrange function of Eq. (39) is represented as

$$L(\mathbf{d}, \alpha) = \mathbf{d}^\top \mathbf{G}(\mathbf{d}) \mathbf{d} + \alpha \sum_{i=1}^K \log(d_i). \quad (40)$$

Let $\nabla L(\mathbf{d}, \alpha) = \frac{\partial L(\mathbf{d})}{\partial \mathbf{d}} = \mathbf{0}_K$, where $\mathbf{0}_K = [0, \dots, 0]^\top$, a system of equations to obtain the optimal of Eq. (40) can be established as

$$\begin{cases} 2\mathbf{G}(\mathbf{d})\mathbf{d} + \mathbf{d}^\top \left(\frac{\partial \mathbf{G}(\mathbf{d})}{\partial \mathbf{d}} \right) \mathbf{d} + \alpha(\mathbf{1}_K \oslash \mathbf{d}) = \mathbf{0}_K; \\ \sum_{i=1}^K \log(d_i) = 0. \end{cases} \quad (41)$$

To solve Eq. (41), it is important to know the mapping $\mathbf{d} \mapsto \mathbf{A}$ and $\mathbf{A} \mapsto \mathbf{d}$. By observing Eq. (22), $\mathbf{d} \mapsto \mathbf{A}$ is related to solve SIVP, which can be calculated by

$$\mathbf{A} = \left(\mathbf{M}^{\frac{1}{2}} \text{diag}(\mathbf{d}) \right)^{-1} \Psi \left(\mathbf{M}^{\frac{1}{2}} \text{diag}(\mathbf{d}) \right), \quad (42)$$

where function $\Psi(\cdot)$ represents the process on solving SIVP. Under a constant \mathbf{M} , \mathbf{d} maps to \mathbf{D} one-by-one, and affects \mathbf{A} by scaling the basis vector in generator matrix $\mathbf{M}^{\frac{1}{2}}$. Regarding the continuity on $\mathbf{d} \mapsto \mathbf{A}$, since SIVP is NP-hard [30] and the solving algorithms (LLL, SD, etc.) are iterative, it is hard to formulate $\mathbf{A} \mapsto \mathbf{d}$ directly, but some law is easily obtained on the \mathbf{A} derived by a vector and its neighborhood in Ω . To describe the similarity between two matrices, we apply the spectral norm $\|\cdot\|_2$ [40] which is defined as

$$\|\mathbf{D}\|_2 \triangleq \sup_{\mathbf{x} \neq \mathbf{0}_K} \frac{\|\mathbf{D}\mathbf{x}\|_2}{\|\mathbf{x}\|_2}. \quad (43)$$

$\|\cdot\|_2$ is a matrix norm compatible with the vector 2-norm. Then, we have a theorem about two similar matrices.

Theorem 1. *Considering a non-singular generator matrix \mathbf{G}_A of lattice Λ_A and a positive diagonal matrix \mathbf{D}_A with constraint $\det(\mathbf{D}_A) = 1$, the product $\mathbf{G}_B = \mathbf{G}_A \mathbf{D}_A$ is the generator matrix of lattice Λ_B , and the solution set of $\Psi(\mathbf{G}_A)$ and $\Psi(\mathbf{G}_B)$ are denoted as \mathcal{S}_A and \mathcal{S}_B respectively. When \mathbf{D}_A is similar to \mathbf{I} , i.e., for a minimum value $\epsilon > 0$, $\|\mathbf{D}_A - \mathbf{I}\|_2$ satisfies*

$$\|\mathbf{D}_A - \mathbf{I}\|_2 < \epsilon, \quad (44)$$

and

$$|\lambda_K(\Lambda_A) - \lambda_K(\Lambda_B)| < \epsilon, \quad (45)$$

so we have

$$\forall \mathbf{R}_B = \mathbf{G}_B \mathbf{U} \in \mathcal{S}_B, \exists \mathbf{R}_A = \mathbf{G}_A \mathbf{V} \in \mathcal{S}_A, \text{ s.t., } \mathbf{U} = \mathbf{V}. \quad (46)$$

Proof. See Appendix A. □

According to Theorem 1, when \mathbf{d} moves at a minimal scale in Ω , \mathbf{A} may remain the same before and after moving only if the successive minima remain continuity. In general, it is hard to delimit when \mathbf{A} is shifted during \mathbf{d} changing, so we take a sample on LLL algorithm in a 2-dimensional basis matrix $\mathbf{M}'_2 = \mathbf{M}_2^{\frac{1}{2}}$. We will introduce this sample in the size reduction condition and Lovász condition.

- *Size reduction condition:* Considering the QR decomposition

$$\mathbf{M}'_2 = \mathbf{Q}_2 \mathbf{R}_2 = \mathbf{Q}_2 \begin{bmatrix} r_{1,1} & r_{1,2} \\ 0 & r_{2,2} \end{bmatrix}. \quad (47)$$

According to Alg. 1, the coefficient of size reduction $\mu = \lfloor \frac{r_{1,2}}{r_{1,1}} \rfloor$ when $\mathbf{D}_2 = \mathbf{I}_2$. For a changed $\mathbf{D}_2 = \text{diag}(d_1, d_2)$, the changed coefficient of size reduction μ' is given by

$$\mu' = \left\lfloor \frac{d_2 r_{1,2}}{d_1 r_{1,1}} \right\rfloor \stackrel{d_1 = \frac{1}{d_2}}{=} \left\lfloor \mu + \left[(d_2^2 - 1) \frac{r_{1,2}}{r_{1,1}} \right] \right\rfloor. \quad (48)$$

When $\left[(d_2^2 - 1) \frac{r_{1,2}}{r_{1,1}} \right] \neq 0$, $\mu' \neq \mu$, such that \mathbf{A}_2 has been changed.

- *Lovász condition:* According to Eq. (25), the swapping between two vector in \mathbf{M}'_2 is related to μ . Since μ has been changed under different \mathbf{D}_2 in size reduction, the number of iterations becomes unknown for the algorithm process in practical, which triggers a sudden changes on $\Psi(\mathbf{M}'_2 \mathbf{D}_2)$ and leads to a different \mathbf{A}_2 .

Based on the above content, we learn that the mapping in Eq. (42) is non-surjective, which reveals the mapping $\mathbf{A} \mapsto \mathbf{d}$ is one-to-many. It explains a possible that each fixed \mathbf{A} corresponds to a region $\mathcal{P}(\mathbf{A})$ of Ω , and these regions form Ω without overlap. We can solve Eq. (41) by dividing Ω into multiple region represented by different \mathbf{A} .

Based on Theorem 1, we have the Theorem 2 for its computational complexity.

Theorem 2. *Solving Eq. (41) is at least NP-hard.*

Proof. Based on the non-surjective in mapping Eq. (42), To solve Eq. (41) is equivalent to solve four continuous subproblems:

- SP1 Without the range constraint of a region $\mathcal{P}(\mathbf{A}_i)$, how to derive the optimal \mathbf{D} of that fixed \mathbf{A}_i ?
- SP2 With the range constraint of a region $\mathcal{P}(\mathbf{A}_i)$, is that optimal \mathbf{D} is within $\mathcal{P}(\mathbf{A}_i)$?
- SP3 The region $\mathcal{P}(\mathbf{A}_i)$ where the optimal \mathbf{D} within $\mathcal{P}(\mathbf{A}_i)$ is referred to as a candidate \mathcal{P} , how to select all candidate \mathcal{P} from all $\mathcal{P}(\mathbf{A})$?
- SP4 How to select the optimal \mathcal{P} from all candidate \mathcal{P} ?

Considering SP2, an effective method is to calculate the \mathbf{A} by the derived optimal \mathbf{D} , and compare the calculated \mathbf{A} with the original \mathbf{A}_i . The process of this method is equivalent to solve SIVP which is NP-hard [30]. Assuming the solutions of SP1, SP3 and SP4 are both polynomial, the whole computational complexity can be derived as

$$T_{\text{whole}} = T_{\text{SP1}} \oplus T_{\text{SP2}} \oplus T_{\text{SP3}} \oplus T_{\text{SP4}} = \text{P} \oplus \text{NP-hard} \oplus \text{P} \oplus \text{P} = \text{NP-hard}. \quad (49)$$

Thus, solving Eq. (41) is at least NP-hard, the theorem is proved. \square

Remark 1. *The same unproven statement in Theorem 2 is mentioned in [20], [22], [25]. Based on Theorem 2, the closed-form solution of Eq. (41) is impossible to obtain unless $P = NP$, which leads us to achieve an approximate solution balanced between complexity and accuracy. In the four subproblems in Theorem 2, SP1's solution is polynomial as the mention in Sect. III-B. Meanwhile, solving SP4 under SP3's solution is equivalent to solve a sequencing problem which is polynomial. The SIVP solver for SP2 is well-studied in [32], [33], [41]. Thus, the difficulty to solve Eq. (41) is how to solve SP3 and SP4.*

B. Model on Fixed \mathbf{A}

Regarding a region represented by a fixed \mathbf{A} , the mapping $\mathbf{d} \mapsto \mathbf{A}$ can be ignored since \mathbf{A} is regarded as a constant integer-value matrix. In this situation, the problem of finding a optimal \mathbf{d} is denoted by

$$\begin{aligned} \arg \min_{\mathbf{d}} \quad & \mathbf{d}^T ((\mathbf{A}\mathbf{A}^T) \circ \mathbf{M}) \mathbf{d}, \\ \text{subject to} \quad & \mathbf{d} \in \Omega, \end{aligned} \quad (50)$$

where the interference coupling matrix $\mathbf{G} = (\mathbf{A}\mathbf{A}^T) \circ \mathbf{M}$ is constant in this situation. The following lemma for the convexity of Eq. (50).

Lemma 1. *Given a fixed \mathbf{A} , Eq. (50) is a convex problem if and only if any of the following conditions are satisfied:*

- i) $N \geq K$ in DIF,
- ii) any $\mathbf{H}^{K \times N}$ in RIF.

Proof. Since the difference of \mathbf{M} in DIF and RIF, we will elaborate these two situations respectively.

- *DIF:* According to Eq. (19), $\mathbf{M} = (\mathbf{H}\mathbf{H}^T)^{-1}$. According to the features of Gram matrix, $\mathbf{H}\mathbf{H}^T$ is semi-positive definite matrix (SPDM), and $\mathbf{A}\mathbf{A}^T$ is positive definite matrix (PDM) since \mathbf{A} is full-rank. When $N \geq K$, $(\mathbf{H}\mathbf{H}^T)^{-1}$ exists and is also SPDM. Based on Schur Product Theorem, $(\mathbf{A}\mathbf{A}^T) \circ \mathbf{M}$ is SPDM, which reveals that the target function in DIF is convex.
- *RIF:* Regarding the singular value decomposition (SVD) of $\mathbf{H}\mathbf{H}^T = \mathbf{Q}\mathbf{\Lambda}\mathbf{Q}^T$, we have

$$\frac{K}{\rho} \mathbf{I} + \mathbf{H}\mathbf{H}^T = \mathbf{Q} \left(\frac{K}{\rho} \mathbf{I} + \mathbf{\Lambda} \right) \mathbf{Q}^T. \quad (51)$$

Since $\frac{K}{\rho} > 0$, $\frac{K}{\rho} \mathbf{I} + \mathbf{H}\mathbf{H}^T$ is a PDM. Similar to DIF, $\mathbf{M} = \left(\frac{K}{\rho} \mathbf{I} + \mathbf{H}\mathbf{H}^T \right)^{-1}$ is the PDM, and $(\mathbf{A}\mathbf{A}^T) \circ \mathbf{M}$ is also the PDM. Thus, the target function in RIF is convex.

Combining the above two points, $\mathbf{d}^\top ((\mathbf{A}\mathbf{A}^\top) \circ \mathbf{M}) \mathbf{d}$ is convex when $N \geq K$ in DIF and any $\mathbf{H}^{K \times N}$ in RIF. The lemma has been proved. \square

To solve Eq. (50), we establish the Lagrange function to

$$L_{\text{fix}}(\mathbf{d}, \alpha) = \mathbf{d}^\top \mathbf{G} \mathbf{d} + \alpha \sum_{i=1}^K \log(d_i), \quad (52)$$

and solve $\nabla L_{\text{fix}}(\mathbf{d}, \alpha) = \mathbf{0}_K$ yielding to

$$\begin{cases} \nabla L_{\text{fix}}(\mathbf{d}, \alpha) = 2\mathbf{G}\mathbf{d} + \alpha(\mathbf{1}_K \oslash \mathbf{d}) = \mathbf{0}_K; \\ \sum_{i=1}^K \log(d_i) = 0. \end{cases} \quad (53)$$

For $\nabla L_{\text{fix}}(\mathbf{d}, \alpha)$, since $\mathbf{d}^\top \mathbf{0}_K = 0$ and $\mathbf{d}^\top (\mathbf{1}_K \oslash \mathbf{d}) = K$, Eq. (53) is equivalent to

$$\begin{cases} \mathbf{d}^\top \mathbf{G} \mathbf{d} = -\frac{\alpha K}{2}; \\ \sum_{i=1}^K \log(d_i) = 0. \end{cases} \quad (54)$$

Based on Lemma 1 that \mathbf{G} is a PDM, the quadratic of \mathbf{G} remains positive, indicating that α is negative. Thus, $\mathbf{d}^\top \mathbf{G} \mathbf{d} = \frac{|\alpha|K}{2}$ can be regarded as a hyperellipsoid in \mathcal{D} conducted from $\mathbf{d}^\top \mathbf{G} \mathbf{d} = 1$ by scaling $\frac{|\alpha|K}{2}$. Furthermore, considering a kind of decomposition that $\mathbf{G} = \mathbf{T}^\top \mathbf{T}$, $\mathbf{d}^\top \mathbf{G} \mathbf{d} = \frac{|\alpha|K}{2}$ can be formulated as

$$\mathbf{d}^\top \mathbf{G} \mathbf{d} = \frac{|\alpha|K}{2} \Rightarrow \|\mathbf{T}\mathbf{d}\|^2 = \frac{|\alpha|K}{2}. \quad (55)$$

In Eq. (50), we want to minimize $\mathbf{d}^\top \mathbf{G} \mathbf{d}$ in \mathcal{D} . According to Eq. (55), the minimum value is $\frac{|\alpha|K}{2}$ which is a scale on $\mathbf{d}^\top \mathbf{G} \mathbf{d} = 1$. So the problem in Eq. (50) is referred to find a minimum scaling value such that the surface of hypersphere $\|\mathbf{T}\mathbf{d}\|^2 = 1$ reach the origin of \mathcal{D} , which is equivalent to find the minimum vector $\mathbf{T}\mathbf{d}$ on the surface of hypersphere $\|\mathbf{T}\mathbf{d}\|^2 = 1$. Thus, a generalized optimization model in fixed \mathbf{A} is established and represented by

$$\begin{cases} \|\mathbf{T}\mathbf{d}\|^2 = \frac{|\alpha|K}{2}; \\ \sum_{i=1}^K \log(d_i) = 0. \end{cases} \quad (56)$$

Considering SVD $\mathbf{G} = \mathbf{T}^\top \mathbf{T} = \mathbf{Q}\mathbf{A}\mathbf{Q}^\top$ and Lower-Diagonal-Lower Transpose (LDL) $\mathbf{O}\mathbf{G}\mathbf{O}^\top = \mathbf{O}\mathbf{T}^\top \mathbf{T}\mathbf{O}^\top = \mathbf{L}\mathbf{\Sigma}\mathbf{L}^\top$ [25], Fig. 2 depicts some samples in 3-dimension on Eq. (56), in which SNR=15dB and

$$\mathbf{H} = \begin{bmatrix} 0.7826 & 0.6097 & 0.7154 \\ 1.8776 & 1.8774 & 0.1899 \\ 1.8507 & 0.0694 & 0.3630 \end{bmatrix}.$$

From the observations of Fig. 2 (a) and (b), the shape of the region transformed by \mathbf{T} (colored in red) has been changed compared to the region of Ω (colored in blue), which causes the extreme for optimization (reconstructed from the shortest vector in red region) offset from the shortest vector in Ω . The deformation on transformed region is caused by two reasons:

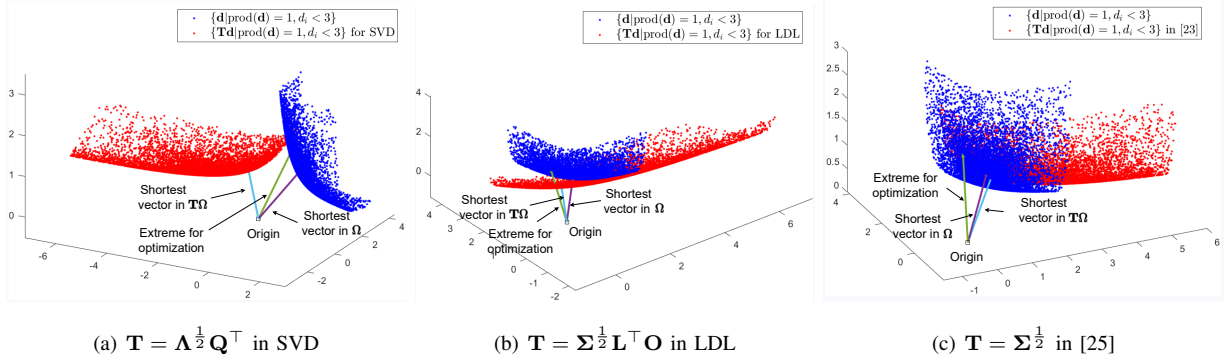


Fig. 2. 3-dimensional sample for generalized optimization model in fixed \mathbf{A}

- i) The rotating caused by unitary matrix changes the spatial location of region, which causes the scaling affected by diagonal matrix partially changes to a folding effects.
- ii) the scaling affected by diagonal matrix makes the boss of Ω tilts to along a certain direction.

Meanwhile, considering LDL and $\mathbf{L}^{\top} \mathbf{O} = \mathbf{I}$, the generalized model in Eq. (56) becomes the method proposed in [25], which is depicted in Fig. 2 (c). From that figure, we can observe that the consideration $\mathbf{L}^{\top} \mathbf{O} = \mathbf{I}$ ignores the rotating caused by unitary matrix, which causes an obvious deviation from the practical optimum.

Remark 2. Since the problem in Eq. (50) is equivalent to find the minimum vector $\mathbf{T}\mathbf{d}$ on the surface of hypersphere $\|\mathbf{T}\mathbf{d}\|^2 = 1$, the points in that hypersphere can be also regarded as the alternative in \mathbf{d} selecting. It reflects that the constraint $\prod_{i=1}^K d_i \leq 1$ is the same as $\prod_{i=1}^K d_i = 1$ in geometric perspective, and obtain the same solution. Due to the equivalence on $\prod_{i=1}^K d_i \leq 1$ and $\sum_{i=1}^K \log(d_i)$, the constrain in Eq. (50) can be shifted to convex in geometric perspective, and the problem in Eq. (50) is convex combining with Lemma 1.

Comprehensive the above contents, we have Theorem 3 for the characteristic of solution set in Eq. (41).

Theorem 3. The solution set \mathcal{S} of Eq. (41) is a finite nonempty set in \mathcal{D} .

Proof. See Appendix B. □

Remark 3. If we regard Ω as a set of $\mathcal{P}(\mathbf{A})$, then searching for the optimal extremum on Ω can be interpreted as a search over the elements of \mathcal{S} . According to Theorem 3, \mathcal{S} is a proper subset of the real number space \mathbb{R}^K , which implies that the search space can be reduced and the time complexity lowered when \mathcal{S} is known, either completely or in part. If \mathcal{S} is fully known, the optimal extremum can be selected from the extrema corresponding to all $\mathcal{P}(\mathbf{A})$ associated with \mathcal{S} ; if only partially known, a sub-optimal extremum can be obtained.

IV. OPTIMAL IF PRECODER DESIGN

To obtain the optimal IF precoder from the proposed generalized model, we proposes a method to optimize (\mathbf{A}, \mathbf{D}) adaptive to the channel matrix \mathbf{H} and SNR, referring to as Multi-Cone Nested Stochastic Pattern Search

(MCN-SPS). In this section, we introduce this method on the optimization for fixed \mathbf{A} (Solving SP1), alternating optimization for (\mathbf{A}, \mathbf{D}) (Solving SP3) and the stochastic pattern.

A. Optimization for Fixed \mathbf{A}

To solve Eq. (56), from Fig. 2, we find that the shape of Ω forms a cone in the holopositive region of \mathcal{D} . We have the following lemma for this hypothesis.

Lemma 2. *To Ω , any ray started from the origin and towards \mathcal{D} 's holopositive region \mathcal{D}^+ have and only have one intersection. For the space \mathcal{B} transformed by \mathbf{B} from \mathcal{D} , this characteristic holds true for $\Omega_2 = \left\{ \mathbf{B}(\mathbf{1}_K \otimes \mathbf{d}) \mid \prod_{i=1}^K d_i = 1, d_i > 0, i \in 1, \dots, K \right\}$, where \mathbf{B} represents arbitrarily non-negative matrix.*

Proof. We prove Lemma 2 by using contradiction. Firstly, we assume

$$\exists \mathbf{r} = [r_1, \dots, r_{K-1}, \beta]^\top \in \mathcal{D}^+ \text{ s.t., } \mathbf{r} \notin \Omega, \text{ and, } \mathbf{B}\mathbf{r} \notin \Omega_2. \quad (57)$$

Since $d_i > 0, i \in 1, \dots, K$, it is impossible to find a \mathbf{r} in the holopositive region of \mathcal{D} with $\beta < 0$. Thus, \mathbf{r} must belong to Ω , and $\mathbf{B}\mathbf{r} \notin \Omega_2$. In other word, any ray toward the holopositive region of \mathcal{D} must have intersection to Ω , and so as for \mathcal{B} to Ω_2 .

Regarding the uniqueness of intersection, since there are two propositions in this lemma, we will prove them respectively.

- Ω : Assuming that there are two intersection for a ray to Ω , i.e.,

$$\forall \mathbf{d}_1 = [d_{1,1}, \dots, d_{1,K}]^\top, \mathbf{d}_2 = \eta \mathbf{d}_1 \in \Omega, \eta \neq 1, \text{ s.t., } \prod_{i=1}^K d_{1,i} = 1, \prod_{i=1}^K d_{2,i} = 1. \quad (58)$$

However, due to

$$\prod_{i=1}^K d_{2,i} = \eta^K \prod_{i=1}^K d_{1,i} = \eta^K, \quad (59)$$

it is contradictory to Eq. (58), and any intersection number more than 2 is contradictory similarly for the same reason. Thus, there is only one intersection between any ray toward the holopositive region of \mathcal{D} and Ω .

- Ω_2 : For any $\mathbf{d} \in \Omega$, when $\prod_{i=1}^K d_i = 1$, we have

$$\prod_{i=1}^K \frac{1}{d_i} = 1 \quad (60)$$

so the set

$$\Omega_3 = \left\{ (\mathbf{1}_K \otimes \mathbf{d}) \mid \prod_{i=1}^K d_i = 1, d_i > 0, i \in 1, \dots, K \right\}. \quad (61)$$

corresponds to Ω one-by-one. Similarly, when we assume that

$$\forall \mathbf{x}_1, \mathbf{x}_2 = \eta \mathbf{x}_1 \in \Omega_2, \eta \neq 1, \text{ s.t., } \prod_{i=1}^K [\mathbf{B}^{-1} \mathbf{x}_1]_i = 1, \prod_{i=1}^K [\mathbf{B}^{-1} \mathbf{x}_2]_i = 1, \quad (62)$$

it is contradictory since

$$\prod_{i=1}^K [\mathbf{B}^{-1} \mathbf{x}_2]_i = \eta^K \prod_{i=1}^K [\mathbf{B}^{-1} \mathbf{x}_1]_i = \eta^K. \quad (63)$$

According the one-by-one corresponding, there is only one intersection between any ray toward the holopositive region of \mathcal{B} and Ω_2 .

Combining aforementioned contents, the lemma has been proved. \square

The Lemma 2 reveals that each $\mathbf{d} \in \Omega$ corresponds to the ray toward the holopositive region of \mathcal{D} , which inspire us that to locate a \mathbf{d} only require the direction of \mathbf{d} rather than its length. Based on this inspiration, obtaining the optimal \mathbf{d} only requires the proportion of each d_i . According to Eq. (53), we have

$$\begin{cases} 2\mathbf{G}\mathbf{d} + \alpha(\mathbf{1}_K \oslash \mathbf{d}) = \mathbf{0}_K \\ \sum_{i=1}^K \log(d_i) = 0 \end{cases} \Rightarrow \begin{cases} d_1 \mathbf{g}_1^\top \mathbf{d} = -\frac{\alpha}{2} \\ \dots \\ d_K \mathbf{g}_K^\top \mathbf{d} = -\frac{\alpha}{2} \\ \sum_{i=1}^K \log(d_i) = 0 \end{cases}, \quad (64)$$

where $\mathbf{g}_i, i \in \{1, \dots, K\}$ represents the row of \mathbf{G} . From Eq. (64), we find $d_1 \mathbf{g}_1^\top \mathbf{d} = \dots = d_K \mathbf{g}_K^\top \mathbf{d} = -\alpha/2$, alternatively,

$$\frac{d_i}{d_j} = \frac{\mathbf{g}_j^\top \mathbf{d}}{\mathbf{g}_i^\top \mathbf{d}}, \quad i \neq j. \quad (65)$$

By conducting the auxiliary matrix

$$\mathbf{S} = \begin{bmatrix} \frac{d_1}{d_1} & \dots & \frac{d_1}{d_K} \\ \dots & \ddots & \dots \\ \frac{d_K}{d_1} & \dots & \frac{d_K}{d_K} \end{bmatrix}, \quad (66)$$

the proportion of each d_i can be calculated by

$$\frac{d_j}{\sum_{i=1}^K d_i} = (\mathbf{S}_j^\top \mathbf{1}_K)^{-1} = \left(\frac{d_1}{d_j} + \dots + \frac{d_K}{d_j} \right)^{-1} = \left(\frac{\mathbf{g}_j^\top \mathbf{d}}{\mathbf{g}_1^\top \mathbf{d}} + \dots + \frac{\mathbf{g}_j^\top \mathbf{d}}{\mathbf{g}_K^\top \mathbf{d}} \right)^{-1} = \frac{1}{\mathbf{g}_j^\top \mathbf{d}} \left(\sum_{i=1}^K \frac{1}{\mathbf{g}_i^\top \mathbf{d}} \right)^{-1}. \quad (67)$$

Since $\left(\sum_{i=1}^K \frac{1}{\mathbf{g}_i^\top \mathbf{d}} \right)^{-1}$ is a constant only corresponding to \mathbf{G} , we derive that

$$\mathbf{d}_{\text{opt}} \propto \left[\frac{1}{\mathbf{g}_j^\top \mathbf{d}} \right]_{j \in \{1, \dots, K\}}. \quad (68)$$

Thus, regarding the direction of \mathbf{d} , the equation system for \mathbf{d} optimization is given by

$$\begin{cases} \mathbf{G}\mathbf{d} \propto \mathbf{1}_K \oslash \mathbf{d}; \\ \prod_{i=1}^K d_i = 1. \end{cases} \quad (69)$$

To solve Eq. (69), we can recognize it as a special case of matrix balancing problem. Here we have the following theorem about this equivalence.

Theorem 4. *The constraint $\prod_{i=1}^K d_i = 1$ can be expressed by the scaling function*

$$\Gamma(\mathbf{x}) = \vartheta(\mathbf{x})\mathbf{x}, \quad \vartheta(\mathbf{x}) \triangleq \frac{1}{\prod_{i=1}^K x_i^{\frac{1}{K}}}, \quad \mathbf{x} = [x_1, \dots, x_K]^\top. \quad (70)$$

Let \mathbf{G} as an M matrix [42]. The problem in fixed \mathbf{A} is equivalent to an unilateral matrix balancing problem with row sum constraints.

That is, we seek a diagonal matrix \mathbf{C} such that the matrix $\mathbf{B} = \vartheta(\mathbf{G}^{-1}\mathbf{C} \cdot \mathbf{1}_K)\mathbf{C}\mathbf{G}^{-1}\mathbf{C}$ is row stochastic, i.e., it satisfy [43]:

$$\mathbf{B} \cdot \mathbf{1}_K = \mathbf{1}_K. \quad (71)$$

Proof. Due to the constrain $\prod_{i=1}^K d_i = 1$, Eq. (69) can be merged into

$$\mathbf{d} = \Gamma(\mathbf{G}^{-1}(\mathbf{1}_K \otimes \mathbf{d})) = \vartheta(\mathbf{G}^{-1}(\mathbf{1}_K \otimes \mathbf{d}))\mathbf{G}^{-1}(\mathbf{1}_K \otimes \mathbf{d}). \quad (72)$$

The above equation can be reformulated as

$$\begin{aligned} \mathbf{d} &= \vartheta(\mathbf{G}^{-1}(\mathbf{1}_K \otimes \mathbf{d}))\mathbf{G}^{-1}(\mathbf{1}_K \otimes \mathbf{d}) \\ \Rightarrow \mathbf{D} \cdot \mathbf{1}_K &= \vartheta(\mathbf{G}^{-1}\mathbf{D}^{-1} \cdot \mathbf{1}_K)\mathbf{G}^{-1}\mathbf{D}^{-1} \cdot \mathbf{1}_K \\ \Rightarrow \vartheta(\mathbf{G}^{-1}\mathbf{D}^{-1} \cdot \mathbf{1}_K)\mathbf{D}^{-1}\mathbf{G}^{-1}\mathbf{D}^{-1} \cdot \mathbf{1}_K &= \mathbf{1}_K. \end{aligned} \quad (73)$$

Considering $\mathbf{C} = \mathbf{D}^{-1}$, we have

$$\vartheta(\mathbf{G}^{-1}\mathbf{C} \cdot \mathbf{1}_K)\mathbf{C}\mathbf{G}^{-1}\mathbf{C} \cdot \mathbf{1}_K = \mathbf{1}_K. \quad (74)$$

Since \mathbf{G} is an M matrix and is PDM in Lemma 1, \mathbf{G}^{-1} must be a non-negative matrix according to [42]. Considering the matrix $\mathbf{B} = \vartheta(\mathbf{G}^{-1}\mathbf{C} \cdot \mathbf{1}_K)\mathbf{C}\mathbf{G}^{-1}\mathbf{C}$, Eq. (74) can be reformulated as $\mathbf{B} \cdot \mathbf{1}_K = \mathbf{1}_K$. As the non-negative characteristic of \mathbf{G}^{-1} and \mathbf{D} , \mathbf{B} is a non-negative matrix, which also be a row stochastic matrix because the definition in [43]. \square

With Theorem 4, we learn that the \mathbf{D} optimization in fixed \mathbf{A} can be regarded as an unilateral matrix balancing problem with row sum constraints. Inspired by the Sinkhorn iteration [44], the function is formulated as

$$\mathbf{d}^{(t+1)} = \Gamma\left(\mathbf{G}^{-1}\left(\mathbf{1}_K \otimes \mathbf{d}^{(t)}\right)\right), \quad (75)$$

where $\Gamma(\mathbf{x}) = \frac{\mathbf{x}}{\prod_{i=1}^K x_i^{\frac{1}{K}}}$, $\mathbf{x} = [x_1, \dots, x_K]^\top$ is a normalized function to satisfy the constraint $\prod_{i=1}^K d_i = 1$ and t denotes the index of iteration. The convergence of Eq. (75) is proved in the next theorem.

Theorem 5. *Towards the p -PAM symbols in Rayleigh channel, if $\mathbf{A}\mathbf{A}^\top$ is non-negative, Eq. (75) is converged in direction, i.e.,*

$$\mathbf{d}^{(t)} \xrightarrow[t \rightarrow \infty]{} \Gamma\left(\mathbf{G}^{-1}\left(\mathbf{1}_K \otimes \mathbf{d}^{(t)}\right)\right). \quad (76)$$

The aforementioned conclusion holds true in RIF, and in DIF when $N \geq K$.

Proof. See Appendix C. \square

Besides the convergence, Theorem 4 and Theorem 5 reveal some features of Eq. (75):

- i) When \mathbf{G} is a M matrix, its inverse \mathbf{G}^{-1} is a non-negative matrix, ensuring that the $\mathbf{d}^{(t)}$ in t -th iteration is belong to Ω without any modifying.

Algorithm 2 Reciprocal Approximation (RA)**Input:** Channel coefficient matrix \mathbf{H} , SNR ρ , integer coefficient matrix \mathbf{A} , tolerance ϵ **Output:** Optimal power allocation matrix \mathbf{D}

```

1:  $[N, K] \leftarrow \text{size}(\mathbf{H})$ 
2:  $\mathbf{M} \leftarrow \left( \frac{K}{\rho} \mathbf{I} + \mathbf{H}\mathbf{H}^\top \right)^{-1}$ 
3:  $\mathbf{G} \leftarrow (\mathbf{A}\mathbf{A}^\top) \circ \mathbf{M}$ 
4:  $\mathbf{D} \leftarrow \text{Init}(\mathbf{G})$  ▷ Initialize diagonal matrix
5:  $\text{ang} \leftarrow +\infty$ 
6: while  $\text{ang} > \epsilon$  do
7:    $\mathbf{d}_{\text{old}} \leftarrow \mathbf{D}\mathbf{1}_K$ 
8:    $\mathbf{d}_{\text{new}} \leftarrow \Gamma(\mathbf{G}^{-1}(\mathbf{1}_K \otimes \mathbf{d}_{\text{old}}))$ 
9:    $\mathbf{D} \leftarrow \text{diag}(\mathbf{d}_{\text{new}})$ 
10:   $\text{ang} \leftarrow \log \left( \frac{\max(\mathbf{d}_{\text{new}} \otimes \mathbf{d}_{\text{old}})}{\min(\mathbf{d}_{\text{new}} \otimes \mathbf{d}_{\text{old}})} \right)$ 
11: end while

```

ii) When \mathbf{G} is not a M matrix, according to the Perron-Frobenius Theory with Hilbert metric, the constriction factor γ enlarges and, in the last iteration, remains 1 rather than any values greater than 1, which fixes the ray in two near optimal directions. This feature ensures the effectiveness of optimization.

The optimization under fixed \mathbf{A} can be summarized by Algorithm 2, referred to as Reciprocal Approximation (RA). In this algorithm, Eq. (75) is applied iteratively to transform the reciprocal space into \mathcal{D} , continuously contracting the solution toward a fixed point within \mathcal{D} . The process completes when the Hilbert metric between successive iterates becomes smaller than a given threshold, and the optimal power allocation matrix \mathbf{D} is returned.

Regarding Eq. (75), based on Theorem 4, there are several conditions to ensure the effectiveness of non-negative matrix constraint for matrix balancing problem:

i) channel hardening effect happening: When $N \gg K$, according to random matrix theory [45], the Gram matrix $\mathbf{H}\mathbf{H}^\top$ can be regarded as a diagonal matrix. Since the positive definiteness proved in Lemma 1, the main diagonal elements of $\mathbf{M} = [m_{i,j}]_{i,j \in \{1, \dots, K\}}$ is positive and the others are zero, which is represented by

$$m_{i,j} = \begin{cases} m_{i,j} > 0, & i = j; \\ 0, & i \neq j. \end{cases} \quad (77)$$

Then, since $\mathbf{A}\mathbf{A}^\top$ is SPDM, we have

$$g_{i,j} = \begin{cases} a'_{i,j} \times m_{i,j}, & i = j; \\ 0, & i \neq j. \end{cases} \quad (78)$$

where $a'_{i,j}$ denotes the $\{i, j\}$ elements of $\mathbf{A}\mathbf{A}^\top$ and $g_{i,j}$ the $\{i, j\}$ elements of \mathbf{G} . Eq. (78) reflects that \mathbf{G} is a M matrix [42] whose main diagonal elements is non-negative and the others non-positive. Combining the properties of

M Matrices [42] and \mathbf{G} 's positive definiteness proved in Lemma 1, we learn that \mathbf{G}^{-1} is a positive transformation and conforms to the famous Perron Theorem [36].

We have the following theorem for the approximate solution of Eq. (69) when \mathbf{M} is a diagonal matrix.

Theorem 6. *When \mathbf{M} is a diagonal matrix, a solution of Eq. (69) is given by*

$$\mathbf{D}_{\text{opt}} = \frac{\mathbf{L}^{\frac{1}{2}}}{\det(\mathbf{L})^{\frac{1}{2K}}}, \quad (79)$$

where

$$\mathbf{L} = \text{diag} \left([(\mathbf{A}\mathbf{A}^\top) \circ \mathbf{M}]^{-1} \cdot \mathbf{1}_K \right). \quad (80)$$

Proof. Since \mathbf{M} is a diagonal matrix, it follows Eq. (77). By substituting Eq. (78) into Eq. (69), we have

$$\begin{cases} \begin{bmatrix} d_1 g_{1,1} & \cdots & 0 \\ \cdots & \ddots & \cdots \\ 0 & \cdots & d_K g_{K,K} \end{bmatrix} \mathbf{1}_K \propto \begin{bmatrix} d_1^{-1} & \cdots & 0 \\ \cdots & \ddots & \cdots \\ 0 & \cdots & d_K^{-1} \end{bmatrix} \mathbf{1}_K; \\ \prod_{i=1}^K d_i = 1, \quad i \in \{1, \dots, K\}. \end{cases} \quad (81)$$

After solving Eq. (81), we can derive that

$$\begin{cases} d_1 = \left(\prod_{i=1}^K g_{i,i}^{-\frac{1}{2K}} \right) g_{1,1}^{-\frac{1}{2}}; \\ \cdots \\ d_K = \left(\prod_{i=1}^K g_{i,i}^{-\frac{1}{2K}} \right) g_{K,K}^{-\frac{1}{2}}, \end{cases} \Rightarrow \mathbf{D}_{\text{opt}} = \frac{(\text{diag}(\mathbf{G}^{-1} \cdot \mathbf{1}_K))^{\frac{1}{2}}}{\det(\text{diag}(\mathbf{G}^{-1} \cdot \mathbf{1}_K))^{\frac{1}{2K}}}. \quad (82)$$

Since $\mathbf{G} = (\mathbf{A}\mathbf{A}^\top) \circ \mathbf{M}$, the theorem is proved. \square

ii) DIF with LLL algorithm: When $N \geq K$, DIF employs $\mathbf{M} = (\mathbf{H}\mathbf{H}^\top)^{-1}$ which is a M matrix according to Appendix C. Since \mathbf{H} is with Rayleigh distribution, \mathbf{M} is not a sparse matrix which causes period-2 oscillation in iterative. According to Lemma 3, the transforming matrix to reduce the basis $\mathbf{M}^{\frac{1}{2}}\mathbf{D}$ in size reduction condition is non-negative. Since the swapping matrix in Lovász condition is non-negative too, the unimodular matrix \mathbf{A} outputted by LLL algorithm in this situation is non-negative, which meets to the condition that $\mathbf{A}\mathbf{A}^\top$ is non-negative in Theorem 5.

Lemma 3. *In LLL algorithm, the coefficients $\mu_{i,j}$ of size reduction is always non-positive in iteration when the inputted basis $\mathbf{B} = [\mathbf{b}_1, \dots, \mathbf{b}_K]$ satisfies that $\mathbf{B}^\top\mathbf{B}$ is a dense M matrix.*

Proof. We proof this lemma by induction. Since $\mathbf{B}\mathbf{B}^\top$ is a dense M matrix, its non-major diagonal elements are non-positive, which means

$$\mathbf{b}_i^\top \mathbf{b}_j \leq 0, \quad i \neq j. \quad (83)$$

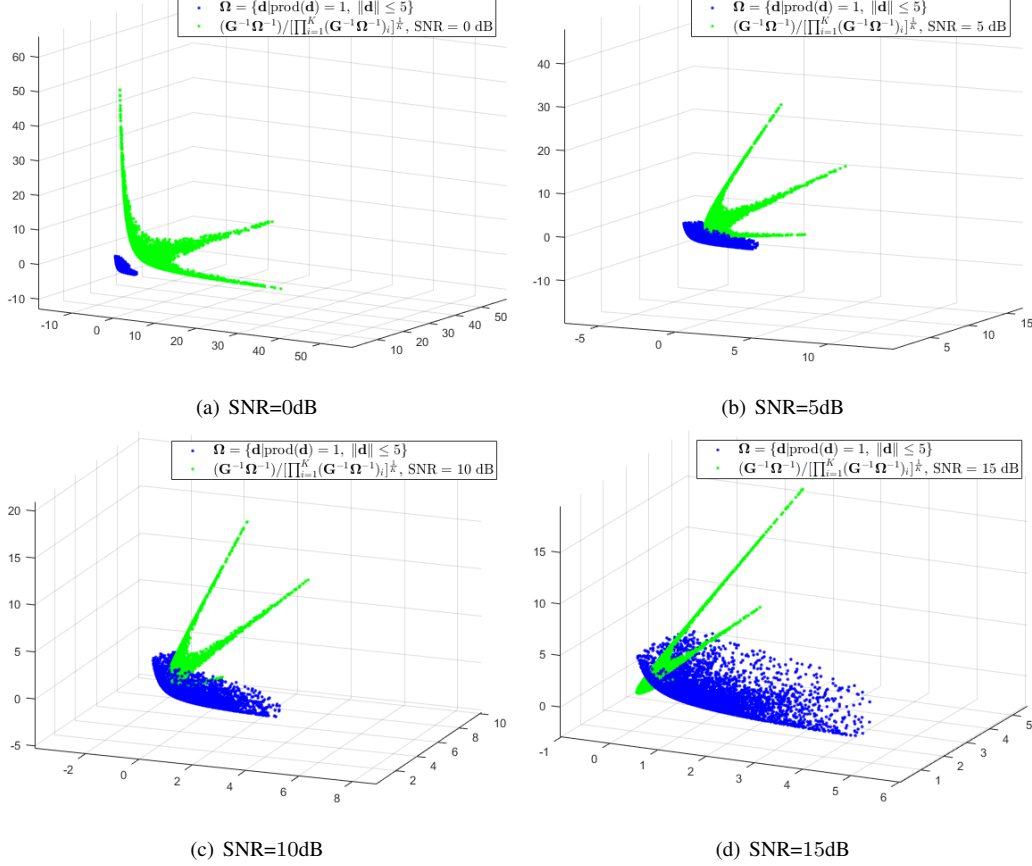


Fig. 3. 3-dimensional sample for the convergence of Eq. (75) versus SNR

After Gram-Schmidt Orthogonalization step in LLL algorithm, we obtain the orthogonal vector $\mathbf{b}_1^*, \dots, \mathbf{b}_K^*$, and $\mathbf{b}_1^* = \mathbf{b}_1$. When $i = 2$, $\mu_{2,1}$ is given by

$$\mu_{2,1} = \frac{\mathbf{b}_2^\top \mathbf{b}_1^*}{(\mathbf{b}_1^*)^\top \mathbf{b}_1^*} = \frac{\mathbf{b}_2^\top \mathbf{b}_1}{\mathbf{b}_1^\top \mathbf{b}_1} \leq 0. \quad (84)$$

By assuming $\forall j < p < i$, $\mu_{p,j} \leq 0$, for $i > j$, we have

$$\mathbf{b}_i^\top \mathbf{b}_j^* = \mathbf{b}_i^\top \mathbf{b}_j - \sum_{p=1}^{j-1} \mu_{p,j} (\mathbf{b}_i^\top \mathbf{b}_p^*). \quad (85)$$

Since $\mu_{p,j} \leq 0$ and $\mathbf{b}_i^\top \mathbf{b}_p^* \leq 0$, $\sum_{p=1}^{j-1} \mu_{p,j} (\mathbf{b}_i^\top \mathbf{b}_p^*) \geq 0$, so $\mathbf{b}_i^\top \mathbf{b}_j^* \leq \mathbf{b}_i^\top \mathbf{b}_j \leq 0$. Thus, we have

$$\mu_{i,j} = \frac{\mathbf{b}_i^\top \mathbf{b}_j^*}{(\mathbf{b}_j^*)^\top \mathbf{b}_j^*} \leq 0. \quad (86)$$

The lemma is proved. \square

iii) RIF with LLL algorithm in high SNR: When SNR is higher enough, $\frac{K}{\rho} \mathbf{I}$ is too small to be ignored, which reveals

$$\mathbf{M} = \left(\frac{K}{\rho} \mathbf{I} + \mathbf{H}\mathbf{H}^\top \right)^{-1} \xrightarrow{\rho \rightarrow +\infty} (\mathbf{H}\mathbf{H}^\top)^{-1}. \quad (87)$$

Algorithm 3 Alternating Optimization (AO)

Input: Initial power allocation matrix \mathbf{D}_{init} , channel matrix \mathbf{H} , SNR ρ .

Output: Sub-optimal power allocation matrix \mathbf{D} , Sub-optimal integer matrix \mathbf{A} .

```

1:  $\mathbf{A}_{\text{tmp}} \leftarrow \mathbf{I}$ 
2:  $\mathbf{M} \leftarrow \left( \frac{K}{\rho} \mathbf{I} + \mathbf{H}\mathbf{H}^\top \right)^{-1}$ 
3: Obtain  $\mathbf{A}$  from  $\mathbf{D}_{\text{init}}$  via Eq. (42)
4:  $\text{iter} \leftarrow 0$ 
5: while  $\mathbf{A}_{\text{tmp}} \neq \mathbf{A}$  do
6:    $\mathbf{D} \leftarrow \text{RA}(\mathbf{H}, \mathbf{A}, \rho)$  ▷ Solve for  $\mathbf{D}$  with fixed  $\mathbf{A}$ 
7:    $\mathbf{A}_{\text{tmp}} \leftarrow \mathbf{A}$ 
8:   Obtain  $\mathbf{A}$  from  $\mathbf{D}$  via Eq. (42)
9:    $\text{iter} \leftarrow \text{iter} + 1$ 
10:  if  $\text{iter} > \text{max\_iter}$  then
11:    break
12:  end if
13: end while

```

As the same reason in case ii, we learn that the unimodular matrix \mathbf{A} outputted by LLL algorithm in this situation is non-negative, which meets to the condition in Theorem 5. To explore how SNR affects the convergence, we present a 3-dimensional sample in

$$\mathbf{H} = \begin{bmatrix} 0.5472 & 0.1643 & 0.4058 \\ 1.2850 & 0.6481 & 1.1394 \\ 0.5685 & 1.1173 & 0.7982 \end{bmatrix}.$$

The observations on Fig. 3 reveal the fact that the point distribution affected by Eq. (75) shrinks during the SNR enlarging, and Eq. (75) mostly converge in direction when $\text{SNR} \geq 5\text{dB}$.

B. Alternating Optimization for (\mathbf{A}, \mathbf{D})

Having addressed the optimization of \mathbf{D} with a fixed \mathbf{A} , we now consider the joint optimization of (\mathbf{A}, \mathbf{D}) . While an optimal \mathbf{d}_{opt} can be found for a given \mathbf{A} , it is important to note that not all such \mathbf{d}_{opt} lies in the dependent set $\mathcal{P}(\mathbf{A})$. A standard approach to find a $\mathbf{d}_{\text{opt}} \in \mathcal{P}(\mathbf{A})$ is to compute the integer matrix \mathbf{A}' associated with \mathbf{d}_{opt} via an SIVP solver and check if \mathbf{A}' matches the original \mathbf{A} . A key challenge in this joint optimization arises when the current $\mathbf{d}_{\text{opt}} \notin \mathcal{P}(\mathbf{A})$: determining the next starting point for the search.

We tackle this challenge using an alternating optimization (AO) framework. The algorithm is designed with a greedy, proximity-based strategy: the integer matrix \mathbf{A} obtained in one iteration directly initializes the next. Each AO iteration executes two consecutive steps: (S1) Given \mathbf{D} , update \mathbf{A} optimally via the SIVP solver in Eq. (42); (S2) Given this \mathbf{A} , update \mathbf{D} optimally via Alg. 2. This alternating process converges to a stationary point (\mathbf{A}, \mathbf{D}) .

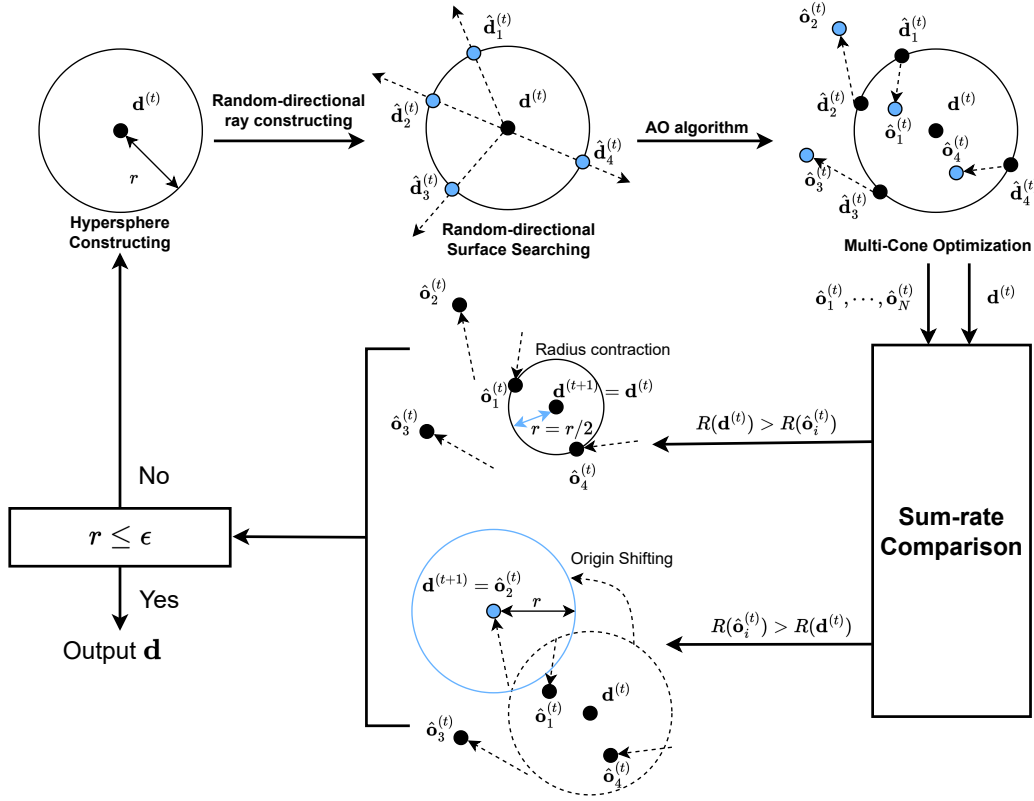


Fig. 4. Flowchart of the MCN-SPS method

Furthermore, because each step is optimal conditional on the other variable, the achievable rate R satisfies the following non-decreasing property at iteration t :

$$R(\mathbf{A}^{(t)}, \mathbf{D}^{(t)}) \leq R(\mathbf{A}^{(t)}, \mathbf{D}_{\text{opt}}^{(t)}) \leq R(\mathbf{A}_{\text{opt}}^{(t)}, \mathbf{D}_{\text{opt}}^{(t)}) = R(\mathbf{A}^{(t+1)}, \mathbf{D}^{(t+1)}). \quad (88)$$

The iteration terminates when

$$\mathbf{A}^{(t)} = \left(\mathbf{M}^{\frac{1}{2}} \mathbf{D}^{(t)} \right)^{-1} \Psi \left(\mathbf{M}^{\frac{1}{2}} \mathbf{D}^{(t)} \right). \quad (89)$$

The overall procedure is summarized in Alg. 3.

C. Multi-Cone Nested Stochastic Pattern Search (MCN-SPS)

If Alg. 3 consistently converged to the unique optimal point $\mathbf{d}_{\text{opt}} \in \mathcal{P}(\mathbf{A})$ within Ω , then the optimal pair (\mathbf{A}, \mathbf{D}) could be readily obtained. However, as indicated by Property 3, this condition is not always met, since multiple disjoint regions may contain such optimal points. To ensure convergence to a globally optimal pair (\mathbf{A}, \mathbf{D}) among these candidate solutions, we propose a method termed the Multi-Cone Nested Stochastic Pattern Search (MCN-SPS). Fig. 4 illustrates the flowchart of the proposed method, which consists of three core processes: search preparation, search and optimization execution, and result integration and adjustment. These three processes are described in detail below.

i) Search preparation: By centering at a $\mathbf{d}^{(t)} \in \Omega$ in the t -th iteration, a hypersphere $\mathcal{B}(\mathbf{d}^{(t)}, r)$ is constructed with a setting radius r . Starting from $\mathbf{d}^{(t)}$, q rays are emitted in stochastic direction, and cross the surface of $\mathcal{B}(\mathbf{d}^{(t)}, r)$ at $\hat{\mathbf{d}}_1^{(t)}, \dots, \hat{\mathbf{d}}_Q^{(t)}$. The i -th intersection $\hat{\mathbf{d}}_i^{(t)}$ can be calculated by

$$\hat{\mathbf{d}}_i^{(t)} = \mathbf{d}^{(t)} + r\hat{\mathbf{v}}_i, \quad (90)$$

where $\hat{\mathbf{v}}_i$ represents the unit vector in the direction of i -th ray. After the movement of $r\hat{\mathbf{v}}_i$, some $\hat{\mathbf{d}}_i^{(t)}$ may leave the holopositive region of \mathcal{D} . To limit in $d_i > 0, i \in \{1, \dots, K\}$, the escaped $\hat{\mathbf{d}}_i^{(t)}$ will be abandoned, and we choose the novel stochastic rays in loop until all vector are limited in the holopositive region of \mathcal{D} .

ii) Search and Optimization execution: After the search space constructing, we correct the intersections $\hat{\mathbf{d}}_1^{(t)}, \dots, \hat{\mathbf{d}}_Q^{(t)}$ to satisfy the constraint by $\Gamma(\cdot)$. Then, these corrected nodes are inputted into Alg. 3 in parallel to obtain their nearby sub-optimal nodes in Ω which satisfies Eq. (89). These nodes, represented as $\hat{\mathbf{o}}_i^{(t)}, i \in 1, \dots, Q$, are the nearby or coincide nodes of $\mathbf{d}^{(t)}$ satisfied $\mathbf{d}_{\text{opt}} \in \mathcal{P}(\mathbf{A})$. To reduce complexity for comparison, we merge the coincide nodes to one node.

iii) Result integration and adjustment: In this operation, we compare the sum rate between $\mathbf{d}^{(t)}$ and its nearby $\hat{\mathbf{o}}_i^{(t)}, i \in 1, \dots, Q$, and adjust the new center in next iteration consisted of two cases:

- i) If any $\hat{\mathbf{o}}_i^{(t)}, i \in 1, \dots, Q$ has the max sum rate, the optimal node is probably located at the vicinity of this nodes. Thus it become the origin of next iteration without other adjustment.
- ii) If $\mathbf{d}^{(t)}$ has the max sum rate compared to $\hat{\mathbf{o}}_i^{(t)}, i \in 1, \dots, Q$, the optimal node seems locate at a region more closer to $\mathbf{d}^{(t)}$. In this case, the radius r is too large to search the nearer region of $\mathbf{d}^{(t)}$, so we contract the radius to $r/2$ and put it into the next iteration.

The iteration is completed when the radius is smaller than a predefined threshold ϵ . The overall procedure is summarized in Alg. 4. Throughout the entire method, the comparisons are implemented in the nodes satisfied $\mathbf{d}_{\text{opt}} \in \mathcal{P}(\mathbf{A})$ which is a finite nonempty discrete set in \mathcal{D} according to Property 3, the search space in the proposed method is smaller than the whole continuous space which is employed in the conventional heuristic algorithm. Thus we achieve a lower complexity with the proposed method, which is demonstrated in the following section.

D. Joint Optimization in Imperfect CSI

According to [20, Theorem 1], DIF precoding achieves maximum spatial multiplexing gain if and only if

$$\mathbf{HP} = \mathbf{DA}. \quad (91)$$

Considering the channel estimation in Eq. (6) and Eq. (7), this principle becomes to

$$(\hat{\mathbf{H}} \pm \mathbf{E})\mathbf{P} = \mathbf{DA}. \quad (92)$$

We can derive the estimation-error-corresponded precoder

$$\mathbf{P} = (\hat{\mathbf{H}} \pm \mathbf{E})^\dagger \mathbf{DA}, \quad (93)$$

Algorithm 4 MCN-SPS method**Input:** Initial power allocation matrix c , channel matrix \mathbf{H} , SNR ρ , Initial step size r_0 **Output:** Optimal power allocation matrix \mathbf{D} , Optimal integer matrix \mathbf{A} .

```

1:  $[N, K] \leftarrow \text{size}(\mathbf{H})$ 
2:  $\mathbf{D} \leftarrow \text{AO}(\mathbf{H}, \mathbf{D}_{\text{init}}, \rho)$ 
3:  $r \leftarrow r_0$ 
4: Obtain  $\mathbf{A}$  from  $\mathbf{D}$  via Eq. (42)
5:  $\mathbf{A}_{\text{tmp}} \leftarrow \mathbf{A}$ 
6: while  $r > \epsilon$  do
7:    $\mathbf{D} \leftarrow \text{AO}(\mathbf{H}, \mathbf{D}, \rho)$ 
8:    $\mathbf{D}_{\text{tmp}} \leftarrow \mathbf{D}$ 
9:   for  $i = 1 : \text{max\_router}$  do ▷ parallel processing
10:      $\mathbf{v} \leftarrow \text{randn}(1, K)$ 
11:      $\mathbf{v} \leftarrow \frac{\mathbf{v}}{\|\mathbf{v}\|}$ 
12:      $\hat{\mathbf{D}}_i \leftarrow \text{diag}(\text{diag} + r\mathbf{v})$ 
13:      $\hat{\mathbf{O}}_i \leftarrow \text{AO}(\mathbf{H}, \hat{\mathbf{D}}_i, \rho)$ 
14:     Obtain  $\hat{\mathbf{A}}_i$  from  $\hat{\mathbf{O}}_i$  via Eq. (42)
15:     if  $R(\hat{\mathbf{A}}_i, \hat{\mathbf{O}}_i) > R(\mathbf{A}, \mathbf{D})$  then
16:        $\mathbf{D}_{\text{tmp}} \leftarrow \hat{\mathbf{O}}_i$ 
17:        $\mathbf{A}_{\text{tmp}} \leftarrow \hat{\mathbf{A}}_i$ 
18:     end if
19:   end for
20:   if  $\mathbf{D}_{\text{tmp}} == \mathbf{D}$  then
21:      $r \leftarrow \frac{r}{2}$ 
22:   end if
23:    $\mathbf{D} \leftarrow \mathbf{D}_{\text{tmp}}$ 
24:    $\mathbf{A} \leftarrow \mathbf{A}_{\text{tmp}}$ 
25: end while

```

where the term ' \dagger ' represents pseudo inverse. However, since $\mathbf{E} \sim \mathcal{N}(0, \sigma_e^2 \mathbf{I})$ is random and σ_e^2 is known, we can estimate a practical precoder under the known σ_e^2 via the MMSE principle defined as

$$\min_{\mathbf{P}} \mathbb{E} [\|\mathbf{HP} - \mathbf{DA}\|_F^2] \Rightarrow \min_{\mathbf{P}} \mathbb{E} \left[\text{Tr} \left((\mathbf{HP} - \mathbf{DA})^\top (\mathbf{HP} - \mathbf{DA}) \right) \right]. \quad (94)$$

Under the MMSE and ML channel estimation, we elaborate the precoder design as following.

i) MMSE: Since there is only one random value $\mathbf{E} \sim \mathcal{N}(0, \sigma_e^2 \mathbf{I})$ in MMSE channel estimation, the target function under MMSE principle is

$$\min_{\mathbf{P}} \mathbb{E}_{\mathbf{E}} [\|\mathbf{HP} - \mathbf{DA}\|_F^2]. \quad (95)$$

Thus, we have a theorem for estimation-error-considered precoder in DIF and RIF.

Theorem 7. *In the MMSE channel estimation when $N \geq K$, considering the channel estimation error $\mathbf{E} \sim \mathcal{N}(0, \sigma_e^2 \mathbf{I})$, the estimation-error-considered precoder $\mathbf{P}_{\text{DIF}}^{\text{MMSE}}$ in DIF is*

$$\mathbf{P}_{\text{DIF}}^{\text{MMSE}} = \frac{1}{\eta} \hat{\mathbf{H}}^\top \left(\hat{\mathbf{H}} \hat{\mathbf{H}}^\top + K \sigma_e^2 \mathbf{I} \right)^{-1} \mathbf{D} \mathbf{A}. \quad (96)$$

In RIF, the precoder is shifted to

$$\mathbf{P}_{\text{RIF}}^{\text{MMSE}} = \frac{1}{\eta} \hat{\mathbf{H}}^\top \left(\hat{\mathbf{H}} \hat{\mathbf{H}}^\top + K \sigma_e^2 \mathbf{I} + \frac{K}{\rho} \mathbf{I} \right)^{-1} \mathbf{D} \mathbf{A}. \quad (97)$$

Proof. See Appendix D. □

ii) ML: Since $\mathbf{H} \sim \mathcal{N}(0, \sigma_h^2) \mathbf{I}$ is independent to $\mathbf{E} \sim \mathcal{N}(\mathbf{0}_K, \sigma_e^2 \mathbf{I})$, according to [46], we derive the conditional distribution that

$$\mathbf{H} | \hat{\mathbf{H}} \sim \mathcal{N} \left(\beta \hat{\mathbf{H}}, \sigma_\xi^2 \mathbf{I} \right), \quad (98)$$

where

$$\beta = \frac{\sigma_h^2}{\sigma_h^2 + \sigma_e^2}, \quad \sigma_\xi^2 = \frac{\sigma_h^2 \sigma_e^2}{\sigma_h^2 + \sigma_e^2}. \quad (99)$$

Considering $\mathbf{H} = \beta \hat{\mathbf{H}} + \boldsymbol{\Xi}$, $\boldsymbol{\Xi} | \hat{\mathbf{H}} \sim \mathcal{N}(\mathbf{0}_K, \sigma_\xi^2 \mathbf{I})$ in ML channel estimation, the target function under MMSE principle is

$$\min_{\mathbf{P}} \mathbb{E}_{\boldsymbol{\Xi} | \hat{\mathbf{H}}} [\|\mathbf{H} \mathbf{P} - \mathbf{D} \mathbf{A}\|_F^2]. \quad (100)$$

Thus, the optimized estimation-error-considered precoder for ML channel estimation is supported in the next theorem.

Theorem 8. *In the ML channel estimation when $N \geq K$, considering the channel estimation error $\mathbf{E} \sim \mathcal{N}(0, \sigma_e^2 \mathbf{I})$ and practical channel $\mathbf{H} \sim \mathcal{N}(0, \sigma_h^2 \mathbf{I})$, the estimation-error-considered precoder $\mathbf{P}_{\text{DIF}}^{\text{ML}}$ in DIF is*

$$\mathbf{P}_{\text{DIF}}^{\text{ML}} = \frac{1}{\eta} \hat{\mathbf{H}}^\top \left(\frac{\sigma_h^2}{\sigma_h^2 + \sigma_e^2} \hat{\mathbf{H}} \hat{\mathbf{H}}^\top + K \sigma_e^2 \mathbf{I} \right)^{-1} \mathbf{D} \mathbf{A}. \quad (101)$$

In RIF, the precoder is shifted to

$$\mathbf{P}_{\text{RIF}}^{\text{ML}} = \frac{1}{\eta} \hat{\mathbf{H}}^\top \left(\frac{\sigma_h^2}{\sigma_h^2 + \sigma_e^2} \hat{\mathbf{H}} \hat{\mathbf{H}}^\top + K \sigma_e^2 \mathbf{I} + \frac{K(\sigma_h^2 + \sigma_e^2)}{\rho \sigma_h^2} \mathbf{I} \right)^{-1} \mathbf{D} \mathbf{A}. \quad (102)$$

Proof. See Appendix E. □

Remark 4. *Inspired by [20], we can easily adapt Eq. (21) and Eq. (22) by regarding \mathbf{P} as $\mathbf{P} = \frac{1}{\eta} \hat{\mathbf{H}}^\top \mathbf{M} \mathbf{D} \mathbf{A}$ when channel estimation error existing. Thus, to adapt the impacts on imperfect CSI, the inputs \mathbf{M} of MCN-SPS method should be shifted according to Theorem 7 and Theorem 8, which are listed at Tab. I.*

V. THEORETICAL ANALYSIS

After introducing the whole method, in this section, we analyze this method theoretically in its complexity and accuracy.

TABLE I
INPUTS \mathbf{M} OF MCN-SPS METHOD WITH ESTIMATION ERROR

Method	MMSE Estimation	ML Estimation
DIF	$\mathbf{M}_{\text{DIF}}^{\text{MMSE}} = (\hat{\mathbf{H}}\hat{\mathbf{H}}^\top + K\sigma_e^2\mathbf{I})^{-1}$	$\mathbf{M}_{\text{DIF}}^{\text{ML}} = \left(\frac{\sigma_h^2}{\sigma_h^2 + \sigma_e^2} \hat{\mathbf{H}}\hat{\mathbf{H}}^\top + K\sigma_e^2\mathbf{I}\right)^{-1}$
RIF	$\mathbf{M}_{\text{RIF}}^{\text{MMSE}} = \left(\hat{\mathbf{H}}\hat{\mathbf{H}}^\top + K\sigma_e^2\mathbf{I} + \frac{K}{\rho}\mathbf{I}\right)^{-1}$	$\mathbf{M}_{\text{RIF}}^{\text{ML}} = \left(\frac{\sigma_h^2}{\sigma_h^2 + \sigma_e^2} \hat{\mathbf{H}}\hat{\mathbf{H}}^\top + K\sigma_e^2\mathbf{I} + \frac{K(\sigma_h^2 + \sigma_e^2)}{\rho\sigma_h^2}\mathbf{I}\right)^{-1}$

A. Computational Complexity Analysis

In our proposed method, the overall procedure of Alg. 4 incorporates an SIVP solver denoted as $\Psi(\cdot)$, whose time complexity is represented as $\mathcal{O}(T_\Psi)$. To analyze the time complexity of the MCN-SPS method, we note that it involves Alg. 3, which itself calls Alg. 2 in a nested manner. Therefore, we evaluate the total time complexity in a layer-by-layer manner. In this section, we consider the inverse calculation for \mathbf{M} obtaining with complexity $\mathcal{O}(K^3)$ in average, and the \mathbf{A} obtaining with $\mathcal{O}(T_\Psi)$.

i) MCN-SPS method (Alg. 4): The whole steps of MCN-SPS method consist of the initialization and iterative steps, which is given by

$$T_{\text{MCN-SPS}} = T_{\text{init},4} + T_{\text{iter},4}. \quad (103)$$

In initialization step, the each assignment is with complexity $\mathcal{O}(1)$, except the initial \mathbf{A} obtaining and the initial \mathbf{D} obtaining with $\mathcal{O}(T_{\text{AO}})$. The whole complexity in initialization step is given by

$$T_{\text{init},4} = \mathcal{O}(T_\Psi) + \mathcal{O}(T_{\text{AO}}). \quad (104)$$

Regarding the iterative steps, since the radius is reduced doubly, the iterative number of the shrinkage step is approach to $\log_2(r_0)$. And we denote the iterative number of origin shifting as $\mathcal{O}(T_{\text{os}})$ which can be regarded as a constant. Inside the iterations, since the operations of each random-directional ray execute in parallel, we ignore the iterative number of the parallel processing. To Eq. (18), it consists of a inverse calculation for \mathbf{M} obtaining. Thus, the whole complexity in iterative steps is given by

$$T_{\text{iter},4} = (\mathcal{O}(T_{\text{AO}}) + \mathcal{O}(T_\Psi) + \mathcal{O}(K^3)) [\log_2(r_0) + \mathcal{O}(T_{\text{os}})]. \quad (105)$$

ii) AO (Alg. 3): The whole steps of AO algorithm consist of the initialization and iterative steps, which is given by

$$T_{\text{AO}} = T_{\text{init},3} + T_{\text{iter},3}. \quad (106)$$

In initialization step, the each assignment is with complexity $\mathcal{O}(1)$, besides once operation for \mathbf{M} and \mathbf{A} obtaining. Thus, we have

$$T_{\text{init},3} = \mathcal{O}(K^3) + \mathcal{O}(T_\Psi). \quad (107)$$

Regarding the iterative steps, the whole iterative number is constrained under a set constant value \max_iter . Inside the iteration, once operation for \mathbf{D} and \mathbf{A} obtaining is implemented on alternating. So $T_{iter,3}$ can be calculated by

$$\begin{aligned} T_{iter,3} &= T_3 (\mathcal{O}(T_{RA} + T_{\Psi})) \\ &\leq \max_iter \times (\mathcal{O}(T_{RA} + T_{\Psi})). \end{aligned} \quad (108)$$

iii) RA (Alg. 2): Regarding the initialization step in Alg. 2, it contains once operation on \mathbf{M} obtaining and \mathbf{D} initialing, where the \mathbf{D} initialing consist of the inverse calculation with complexity $\mathcal{O}(K^3)$ in average. Thus, the complexity of initialization step can be calculated by

$$T_{init,2} = 2\mathcal{O}(K^3). \quad (109)$$

Outside the iterative steps, there is a theorem on the upper bound of iterative number.

Theorem 9. *Under a extreme value ϵ , a interference coupling matrix \mathbf{G} and a initialization $\mathbf{d}^{(0)}$, the iterative number t_{RA} of Alg. 2 satisfies*

$$t_{RA} \leq \frac{\log \epsilon - \log (d_H(\mathbf{G}^{-1}(\mathbf{1}_K \otimes \mathbf{d}^{(0)}), \mathbf{d}^{(0)}))}{\log \left(\tanh \left(\frac{\Delta(\mathbf{G}^{-1})}{4} \right) \right)}, \quad (110)$$

where

$$\Delta(\mathbf{G}^{-1}) = \log \left(\max_{i,j,p,q} \frac{g'_{p,i} g'_{q,j}}{g'_{p,j} g'_{q,i}} \right), \quad (111)$$

and $g'_{i,j}$, $i, j \in \{1, \dots, K\}$ represents the $\{i, j\}$ element of \mathbf{G}^{-1} .

Proof. See Appendix F. □

Regarding the iterative steps, the whole process in each iteration consists a inverse calculation with complexity $\mathcal{O}(K^3)$ to apply Eq. (75) and the others with complexity $\mathcal{O}(K)$. Combining with Theorem 9, the whole complexity of RA algorithm can be calculated by

$$T_{RA} = 2\mathcal{O}(K^3) + t_{RA} (\mathcal{O}(K^3) + 4\mathcal{O}(K)). \quad (112)$$

In combination with the above, since T_3 and T_{os} can be regarded as the constant, we can derive the complexity of our proposed method from

$$\begin{aligned} &T_{MCN-SPS} \\ &= \mathcal{O}((T_{AO} + T_{\Psi} + K^3 + 1)(\log_2(r_0) + T_{os})) \\ &= \mathcal{O}((T_3(T_{RA} + T_{\Psi}) + T_{\Psi} + K^3 + 1)(\log_2(r_0) + T_{os})) \\ &= \mathcal{O}(T_3(T_{\Psi} + t_{RA}K^3)(\log_2(r_0) + T_{os})) \\ &= \mathcal{O}((T_{\Psi} + t_{RA}K^3) \log_2(r_0)). \end{aligned} \quad (113)$$

Considering LLL algorithm for $\Psi(\cdot)$ with complexity $\mathcal{O}(K^4 \log K)$ [12], the proposed method is with complexity $\mathcal{O}(K^4 \log K \log_2(r_0))$. When K enlarge to a tremendously large number such that $K \gg r_0$, $\mathcal{O}(\log_2(r_0))$ can be

TABLE II
THEORETICAL TIME COMPLEXITY IN DIFFERENT SITUATION

Method	Average Complexity	Average Complexity	$K \gg r_0$
		with LLL algorithm	with LLL algorithm
MCN-SPS method	$\mathcal{O}(\log_2(r_0)T_\Psi)$	$\mathcal{O}(K^4 \log K \log_2(r_0))$	$\mathcal{O}(K^4 \log K)$
Venturelli's method [25]	$\mathcal{O}(T_\Psi)$	$\mathcal{O}(K^4 \log K)$	$\mathcal{O}(K^4 \log K)$
PSO-based method [23]	$\mathcal{O}(K^2 T_\Psi)$	$\mathcal{O}(K^6 \log K)$	$\mathcal{O}(K^6 \log K)$

ignored, and the complexity of MCN-SPS method is given by $\mathcal{O}(K^4 \log K)$. In Tab. II, we compare the MCN-SPS method, Venturelli's method [25] and PSO-based method [23] in three cases: the average complexity, average Complexity with LLL algorithm, and $K \gg r_0$ with LLL algorithm. The observations reveal that the MCN-SPS method has a lower complexity in all three cases compared to PSO-based method [23], and approach to an equal complexity on Venturelli's method when $K \gg r_0$.

VI. NUMERICAL VALIDATION OF THEORETICAL FINDINGS

In this section, we evaluate the effectiveness of MCN-SPS method in feasibility, complexity and performance. The simulation setups are summarized as follows.

Metrics: We employ the sum rate and runtime as the metrics of communication performance and complexity respectively, which are obtained by averaging in 1000 Monte-Carlo experiments. The sum rate in each experiment is calculated by Eq. (18). Considering the feasibility verification, we employ the Hilbert metric between this and previous iteration. When the processing is converged into a fixed point, this metric is zero due to the same from input to output. In addition, we define the occupancy of the MIMO system by

$$\text{Occupancy} = \frac{K}{N} \times 100\%, \quad (114)$$

in which the situation of Occupancy $> 100\%$ is referred to as overload MIMO.

Benchmark and setting: In the comparisons, we adopt PSO-based method [23], the [25]'s method, the IF precoding without \mathbf{D} optimization, RZF as the benchmarks, referring to as "PSO", "Venturelli", "Equal Power" and "RZF" respectively. To gain the SIVP solution, we employ LLL algorithm in Alg. 1. In PSO, the maximum of iteration and population size are set as 300 and 50 respectively, and the velocity is within $[-10^{-1}, 10^{-1}]$. Considering Equal Power and RZF, the power allocation matrix \mathbf{D} is both set as \mathbf{I} . To MCN-SPS method, we employ RIF scheme, and set max_iter in Alg. 3 as 100 and r_0 in Alg. 4 as 10. We calculate the upper bound of MIMO system by

$$R_{\text{ub}} = \frac{1}{2} \log \det \left(\mathbf{I} + \frac{\rho}{K} \mathbf{H} \mathbf{W} \mathbf{H}^\top \right), \quad (115)$$

where \mathbf{W} represents the $K \times K$ diagonal matrix outputted by the famous water-filling algorithm [47].

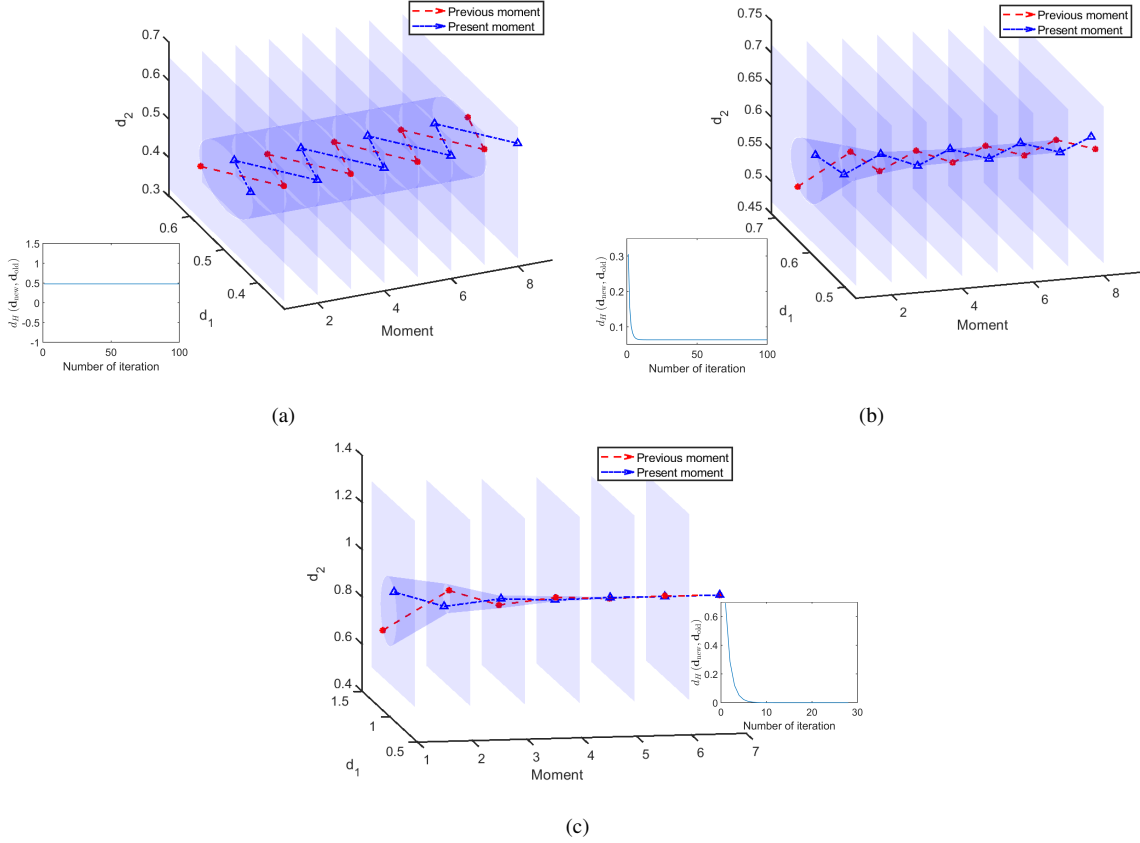


Fig. 5. Trajectory in iterations for the sample \mathbf{H} in: (a) SNR= 0dB, (b) SNR= 5dB, and (c) SNR= 10dB. The trend beside trajectory depicts the Hilbert metric changed in iterations.

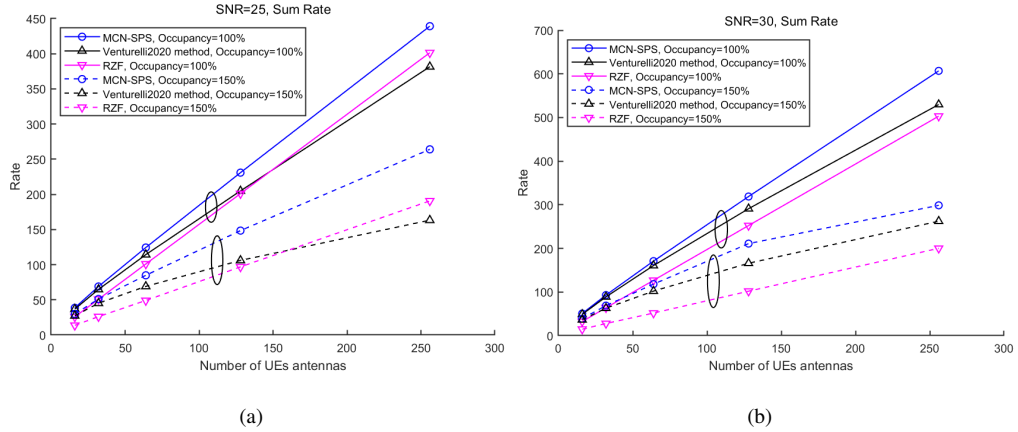


Fig. 6. Sum rate comparisons in different occupancy (100% and 150%) and K (16 to 256) with SNR: (a) 25dB, (b) 30dB.

A. Convergence verification

To verify the convergence, Fig. 5 illustrates the trajectory of the moment vector \mathbf{d} in Ω under a sample channel matrix \mathbf{H} , along with the corresponding trend of the Hilbert metric across iterations, for different SNR values. At SNR= 0dB, a period-2 oscillation is clearly observed in Fig. 5(a): $\mathbf{d}^{(t)}$ jumps between only two positions in Ω ,

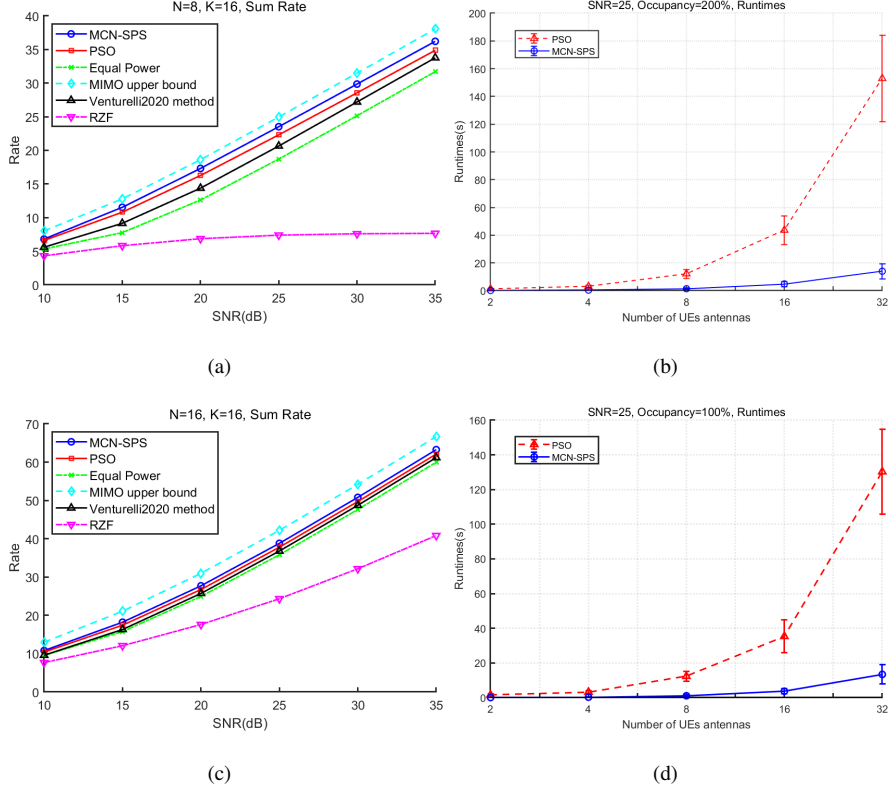


Fig. 7. Sum rate comparisons in different SNR with: (a) $N = 8, K = 16$, (c) $N = K = 16$, and runtime from $K = 2$ to 32 are shown in (b), (d) respectively.

while the Hilbert distance $d_H(\mathbf{d}^{(t+1)}, \mathbf{d}^{(t)})$ remains constant. Geometrically, the cavity in this case appears as a cylinder. In Fig. 5(b), a similar oscillatory behavior persists, but the two locations gradually converge toward each other. This results in a cylindro-conical cavity shape and is reflected in the Hilbert metric, which decreases yet converges to a non-zero value. As the SNR increases further, shown in Fig. 5(c), the cavity takes on a tapered conical form, indicating that the iteration eventually converges. Correspondingly, $d_H(\mathbf{d}^{(t+1)}, \mathbf{d}^{(t)})$ converges to zero. Overall, these observations support the correctness of Lemma 3.

B. Performance comparison

To address the massive communication and ubiquitous application scenarios envisioned for 6G, we conduct a series of comparative experiments to validate the effectiveness and advantages of MCN-SPS in large-scale MIMO systems. Fig. 6 presents the results under different occupancy levels (100% and 150%) and SNR values ranging from 15dB to 30dB. Since the PSO method becomes inapplicable when $K \geq 32$, we compare the sum-rate performance of MCN-SPS, Venturelli's method [25], and RZF for various numbers of user antennas K (from 16 to 256). The following observations can be drawn from Fig. 6:

- i) Across all considered values of K and occupancy levels, MCN-SPS achieves a higher sum-rate compared to all benchmark methods. Moreover, the sum rate gain of MCN-SPS increases as the occupancy level rises, highlighting its applicability in large-scale MIMO systems and its robustness in overloaded MIMO scenarios.

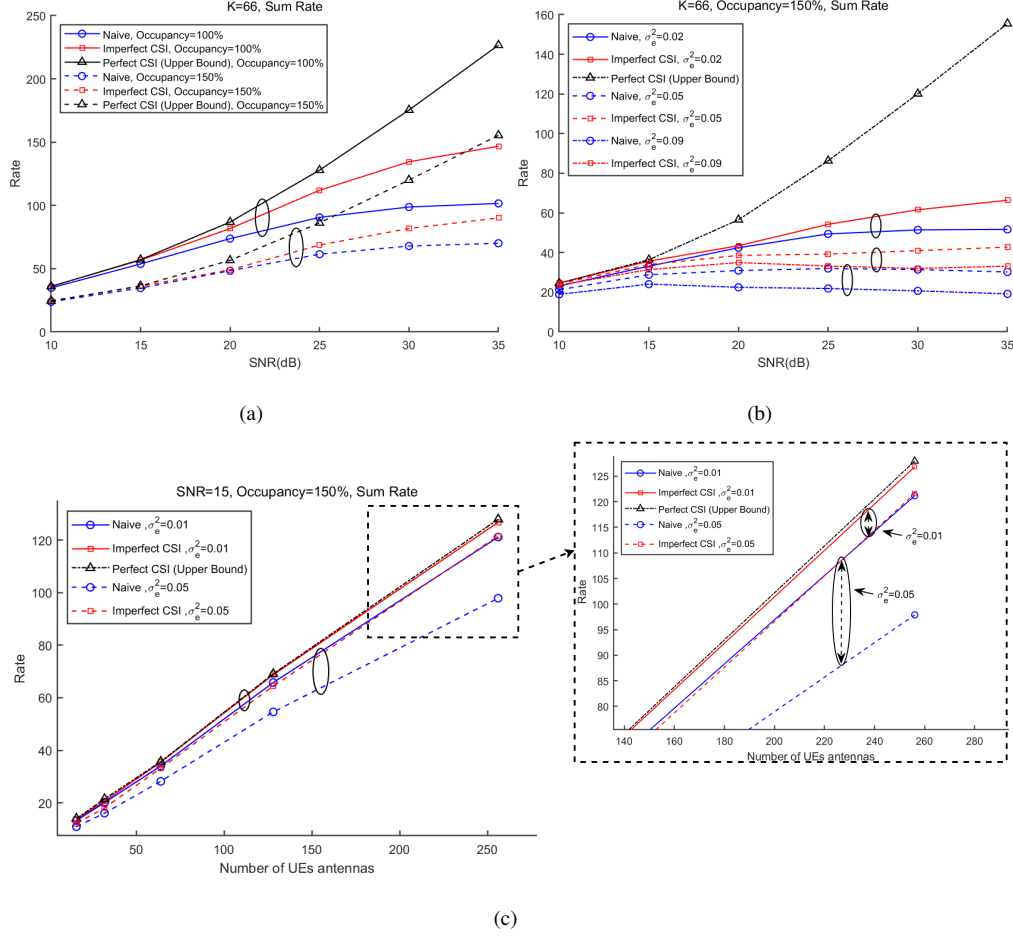


Fig. 8. Sum rate comparisons on the robust precoder designed in Theorem 8 with different: (a) SNR, occupancy, (b) SNR, σ_e^2 , (c) K , σ_e^2 .

- ii) As K grows, the performance gap between MCN-SPS and RZF stabilizes, with their curves becoming nearly parallel. In contrast, the performance of Venturelli's method gradually falls below that of RZF, leading to an intersection between their curves. This indicates that a jointly optimized (\mathbf{A}, \mathbf{D}) pair is crucial for the effectiveness of IF precoding in large-scale MIMO.
- iii) With increasing SNR, the performance gap between MCN-SPS and RZF widens further, while the intersection point between Venturelli's method and RZF shifts toward smaller K . These trends suggest that relaxation-based joint optimization methods for IF precoding exhibit reduced applicability in systems with many users or lower SNR. Such limitations are not observed with MCN-SPS, demonstrating the strong applicability of the MCN-SPS-based IF precoder.

Regarding the performance in different SNR, we establish two comparisons on sum rate and runtime between the proposed method and benchmarks with $N = 8$, $k = 16$ and $N = K = 16$. The results are depicted in Fig. 7, and some observations are obtained as follow.

- i) In overload MIMO depicted in Fig. 7(a), RZF fails to work due to the non-eliminated multi-user interference (MUI). But IF based methods (MCN-SPS, PSO, Venturelli, Equal Power) still work, which reveals RIF have

the effectiveness to reduce MUI.

- ii) Compared to PSO, Venturilli, Equal Power and RZF, our proposed method achieve a higher sum rate in all $\text{SNR} \geq 10\text{dB}$ in Fig. 7(a) and (c), which gain 1dB when $N = K = 16$ and 2dB when $N = 8, k = 16$ compared to PSO method. Meanwhile, the proposed method run in a nearly double lower time compared to PSO method.
- iii) The gap between the upper bound of MIMO system and the proposed method shrinks during the increasing of occupancy, which reveals the applicability of MCN-SPS method in overload MIMO.
- iv) From Fig. 7(b) and Fig. 7(d), MCN-SPS achieves an nearly doubled runtime decreasing compared to PSO, which reflects the lower complexity of MCN-SPS method.

Finally, we evaluate the effectiveness of the robust precoder designed in Theorem 8, which explicitly accounts for channel estimation errors. The results are presented in Fig. 8, which compares the proposed robust design with a conventional (“naive”) approach under different SNRs, occupancy levels (Fig. 8(a)), and estimation-error variances σ_e^2 (Fig. 8(b)). In the naive scheme, the precoder in Eq. (13) and the inputs in Eq. (20) are implemented directly using the estimated channel $\hat{\mathbf{H}}$, without incorporating error statistics. Some observations can be obtained as follow.

- i) Across all subfigures in Fig. 8, the robust precoder of Theorem 8 achieves a higher sum-rate than the naive counterpart, confirming its effectiveness under imperfect CSI for varying SNR, occupancy, and σ_e^2 .
- ii) As shown in Fig. 8(a) and (b), the sum-rate of MCN-SPS increases with SNR, while it decreases with higher occupancy or larger σ_e^2 .
- iii) For a fixed $\sigma_e^2 = 0.02$, the performance gap between the robust and naive schemes widens as SNR increases, yet narrows when the occupancy level rises. While this gap remains approximately constant as σ_e^2 increases across the SNR range, it is more pronounced at lower SNR values and larger numbers of users K .

VII. CONCLUSION

In this paper, a geometry-based generalized optimization model for (\mathbf{A}, \mathbf{D}) optimization. has been proposed. By the proposed generalized model, we find that the solution of (\mathbf{A}, \mathbf{D}) optimization problem can be regarded as the searching on several \mathbf{A} -represented regions independently divided from the whole \mathcal{D} , and each region corresponds the partial of a cone whose points can be represented by the direction of a ray emitted from the origin to \mathcal{D} 's holopositive region. Based on this exploration, a mixed optimization method, referring to as Multi-Cone Nested Stochastic Pattern Search (MCN-SPS) method, has been proposed. The theoretical analysis on complexity shows that the MCN-SPS method achieve a lower complexity of $\mathcal{O}(K^4 \log K \log_2(r_0))$ with LLL algorithm, and reach $\mathcal{O}(K^4 \log K)$ when $K \gg r_0$. The Simulations show that the proposed method features a lower complexity compared with PSO-based method in [23], and gain a higher sum rate compared with all benchmarks.

APPENDIX A
PROOF ON THEOREM 1

We prove Theorem 1 by using contradiction. First, we assume the original proposition does not hold under the original background, i.e., when $\|\mathbf{D}_A - \mathbf{I}\|_2 < \epsilon$ for a minimum value $\epsilon > 0$,

$$\forall \mathbf{R}_B = \mathbf{G}_B \mathbf{U} \in \mathcal{S}_B, \forall \mathbf{R}_A = \mathbf{G}_A \mathbf{V} \in \mathcal{S}_A, \text{ s.t., } \mathbf{U} \neq \mathbf{V}. \quad (116)$$

Since \mathbf{R}_A and \mathbf{R}_B are the SIVP solutions of \mathbf{G}_A and \mathbf{G}_B respectively, based on Definition 2, their basis vectors satisfy

$$\|\mathbf{R}_A \mathbf{e}_i\|_2 = \|\mathbf{G}_A \mathbf{V} \mathbf{e}_i\|_2 \leq \lambda_N(\Lambda_A), \quad (117)$$

$$\|\mathbf{R}_B \mathbf{e}_i\|_2 = \|\mathbf{G}_B \mathbf{U} \mathbf{e}_i\|_2 \leq \lambda_N(\Lambda_B), \quad i \in \{1, \dots, K\}, \quad (118)$$

where \mathbf{e}_i denotes the i -th column of identity matrix \mathbf{I} . Since \mathbf{U} is the unimodular matrix, $\mathbf{G}_A \mathbf{U}$ is also a generator matrix of Λ_A . Due to $\mathbf{G}_B = \mathbf{G}_A \mathbf{D}_A$, we have

$$\mathbf{G}_B \mathbf{U} \mathbf{e}_i - \mathbf{G}_A \mathbf{U} \mathbf{e}_i = \mathbf{G}_A \mathbf{D}_A \mathbf{U} \mathbf{e}_i - \mathbf{G}_A \mathbf{U} \mathbf{e}_i = \mathbf{G}_A (\mathbf{D}_A \mathbf{U} \mathbf{e}_i - \mathbf{U} \mathbf{e}_i). \quad (119)$$

Since $\|\cdot\|_2$ is a matrix norm compatible with the vector 2-norm, we have

$$\|\mathbf{G}_B \mathbf{U} \mathbf{e}_i - \mathbf{G}_A \mathbf{U} \mathbf{e}_i\|_2 = \|\mathbf{G}_A (\mathbf{D}_A \mathbf{U} \mathbf{e}_i - \mathbf{U} \mathbf{e}_i)\|_2 \leq \|\mathbf{G}_A\|_2 \|\mathbf{D}_A \mathbf{U} \mathbf{e}_i - \mathbf{U} \mathbf{e}_i\|_2. \quad (120)$$

Because \mathbf{G}_A is known, $\|\mathbf{G}_A\|_2$ can be regarded as a known value. Meanwhile, since $\|\mathbf{D}_A - \mathbf{I}\|_2 < \epsilon$, we have

$$\|\mathbf{D}_A \mathbf{U} \mathbf{e}_i - \mathbf{U} \mathbf{e}_i\|_2 = \|(\mathbf{D}_A - \mathbf{I}) \mathbf{U} \mathbf{e}_i\|_2 \leq \|\mathbf{D}_A - \mathbf{I}\|_2 \|\mathbf{U} \mathbf{e}_i\|_2 < \epsilon \|\mathbf{U} \mathbf{e}_i\|_2. \quad (121)$$

By regarding $\|\mathbf{U} \mathbf{e}_i\|_2$ a constant, $\|\mathbf{D}_A \mathbf{U} \mathbf{e}_i - \mathbf{U} \mathbf{e}_i\|_2$ is bounded and approach to zero when $\|\mathbf{D}_A - \mathbf{I}\|_2 < \epsilon$, i.e.,

$$\forall \epsilon_2 > 0, \exists \epsilon > 0, \text{ s.t., } \|\mathbf{D}_A - \mathbf{I}\|_2 < \epsilon, \|\mathbf{D}_A \mathbf{U} \mathbf{e}_i - \mathbf{U} \mathbf{e}_i\|_2 < \epsilon_2. \quad (122)$$

Since $\epsilon_2 > 0$ can be any positive minimum value, we assume that $\epsilon_2 = \frac{\epsilon}{\|\mathbf{G}_A\|_2}$, and we have

$$\|\mathbf{G}_B \mathbf{U} \mathbf{e}_i - \mathbf{G}_A \mathbf{U} \mathbf{e}_i\|_2 \leq \|\mathbf{G}_A\|_2 \|\mathbf{D}_A \mathbf{U} \mathbf{e}_i - \mathbf{U} \mathbf{e}_i\|_2 < \|\mathbf{G}_A\|_2 \times \frac{\epsilon}{\|\mathbf{G}_A\|_2} = \epsilon. \quad (123)$$

According to the trigonometric inequality and Eq. (45), we can derive that

$$\begin{aligned} \|\mathbf{G}_A \mathbf{U} \mathbf{e}_i\|_2 &= \|\mathbf{G}_B \mathbf{U} \mathbf{e}_i - (\mathbf{G}_B \mathbf{U} \mathbf{e}_i - \mathbf{G}_A \mathbf{U} \mathbf{e}_i)\|_2 \\ &\leq \|\mathbf{G}_B \mathbf{U} \mathbf{e}_i\|_2 + \|\mathbf{G}_B \mathbf{U} \mathbf{e}_i - \mathbf{G}_A \mathbf{U} \mathbf{e}_i\|_2 \\ &< \lambda_K(\Lambda_B) + \epsilon < \lambda_K(\Lambda_A) + 2\epsilon. \end{aligned} \quad (124)$$

There are two cases for the relationship of $\|\mathbf{G}_A \mathbf{U} \mathbf{e}_i\|_2$ and $\lambda_K(\Lambda_A)$: $\|\mathbf{G}_A \mathbf{U} \mathbf{e}_i\|_2 > \lambda_K(\Lambda_A)$ and $\|\mathbf{G}_A \mathbf{U} \mathbf{e}_i\|_2 \leq \lambda_K(\Lambda_A)$. If $\|\mathbf{G}_A \mathbf{U} \mathbf{e}_i\|_2 > \lambda_K(\Lambda_A)$, we let

$$\exists \mathbf{e}_i, \text{ s.t., } \epsilon \in \left(0, \frac{\|\mathbf{G}_A \mathbf{U} \mathbf{e}_i\|_2 - \lambda_K(\Lambda_A)}{2}\right], \quad (125)$$

so we have

$$\lambda_K(\Lambda_A) + 2\epsilon \in (\lambda_K(\Lambda_A), \|\mathbf{G}_A \mathbf{U} \mathbf{e}_i\|_2]. \quad (126)$$

However, it is contradictory between $\lambda_K(\Lambda_A) + 2\epsilon \leq \|\mathbf{G}_A \mathbf{U} \mathbf{e}_i\|_2$ and Eq. (124), $\|\mathbf{G}_A \mathbf{U} \mathbf{e}_i\|_2 \leq \lambda_K(\Lambda_A)$ hold true for all $\epsilon > 0$. According to the Definition 2, $\mathbf{G}_A \mathbf{U}$ is one of the SIVP solution of Λ_A . There exists a unimodular matrix \mathbf{U} such that $\mathbf{V} = \mathbf{U}$, which is contradictory to Eq. (116). Thus, the original proposition in Theorem 1 is true, and Theorem 1 has been proved.

APPENDIX B PROOF ON THEOREM 3

the characteristic of \mathcal{S} consists of the boundedness, discreteness, finiteness and nonempty property, which we will elaborate them respectively:

i) Boundedness: Since \mathbf{M} is a PDM under the condition in Lemma 1, there must exist a constant $\phi > 0$, s.t.,

$$\mathbf{v}^\top \mathbf{M} \mathbf{v} \geq \phi \|\mathbf{v}\|^2, \quad \forall \mathbf{v} \in \mathbb{R}^K. \quad (127)$$

Considering the target function in Eq. (21), we have

$$\text{Tr}(\mathbf{A}^\top \mathbf{D}^\top \mathbf{M} \mathbf{D} \mathbf{A}) \geq \phi \sum_{i=1}^K \|\mathbf{D} \mathbf{a}_i\|^2, \quad (128)$$

where \mathbf{a}_i represents the i -th column of \mathbf{A} . By the constrain $\prod_{i=1}^K d_i = 1$, we can derive the following solutions:

- 1 when a $d_i \rightarrow 0$, it must have a $d_j \rightarrow \infty$ to remain the constrain.
- 2 when a $d_j \rightarrow 0$, and the j -th parameter of corresponded column \mathbf{a}_i is nonzero, we have $\|\mathbf{D} \mathbf{a}_i\| \rightarrow \infty$, and $\text{Tr}(\mathbf{A}^\top \mathbf{D}^\top \mathbf{M} \mathbf{D} \mathbf{A}) \rightarrow \infty$, which is impossible to as a minimum value of $\text{Tr}(\mathbf{A}^\top \mathbf{D}^\top \mathbf{M} \mathbf{D} \mathbf{A})$.

Thus, it exists a constant C , s.t., $\forall d_i \in [m, M]$, $m > 0$, $M < \infty$ when $\text{Tr}(\mathbf{A}^\top \mathbf{D}^\top \mathbf{M} \mathbf{D} \mathbf{A}) \leq C$, which reveals the boundness of \mathcal{S} .

ii) Discreteness: We prove this property by using contradiction. Firstly, we assume there exists a dissimilarity point sequence $\{(\mathbf{A}_n, \mathbf{d}_n)\} \subset \mathcal{S}$ satisfies

$$(\mathbf{A}_n, \mathbf{d}_n) \rightarrow (\mathbf{A}^*, \mathbf{d}^*). \quad (129)$$

Since \mathbf{A}_n is an integer-valued matrix, it must be $\mathbf{A}_n = \mathbf{A}^*$ when n is larger enough, which leads that \mathbf{d}_n is the solution of Eq. (50). According to Lemma 1 and Remark 2, Eq. (50) can be regarded as a convex problem whose solution represented by $\mathbf{d}_{\mathbf{A}}^*$ is unique [48]. Based on Eq. (42) and Remark 2, any $(\mathbf{A}, \mathbf{d}) \in \mathcal{S}$ requires consistency, which reveals that $(\mathbf{A}^*, \mathbf{d}_{\mathbf{A}}^*) \in \mathcal{S}$. Thus, when n is large enough, $(\mathbf{A}_n, \mathbf{d}_n)$ becomes constant sequence which is contradictory to the definition of dissimilarity point sequence. So it is impossible existing a dissimilarity point sequence consisted in \mathcal{S} , and \mathcal{S} is discrete.

iii) Finiteness: Since \mathcal{S} is a bounded discrete set in finite dimensional Euclidean space, \mathcal{S} is a compact set. According [49, Theorem 2.4.1], \mathcal{S} is a finite set.

iv) Nonempty property: We prove this property by using contradiction. Firstly, we assume that none of regions in Ω have the extreme. Since Ω fulfill the whole \mathbb{R}_+^{K-1} , the problem in Eq. (50) have no solution for every \mathbf{A} , which is contradictory to Lemma 1. Thus, there must be at least one region with extreme, and \mathcal{S} is nonempty.

APPENDIX C
PROOF ON THEOREM 5

Before proving Theorem 5, there is a lemma about the characteristic of Hilbert metric on the vector $\mathbf{1}_K \otimes \mathbf{d}$

Lemma 4. *In the complete metric space with Hilbert metric, we have*

$$\forall \mathbf{d}_x, \mathbf{d}_y \in \mathcal{D}, \text{ s.t.}, d_H(\mathbf{1}_K \otimes \mathbf{d}_x, \mathbf{1}_K \otimes \mathbf{d}_y) = d_H(\mathbf{d}_x, \mathbf{d}_y). \quad (130)$$

Proof. Regarding $\forall \mathbf{d}_x = [d_{x,1}, \dots, d_{x,K}]^\top, \mathbf{d}_y = [d_{y,1}, \dots, d_{y,K}]^\top \in \mathcal{D}$, since the negative correlation of reciprocal, we have

$$\begin{aligned} & d_H(\mathbf{1}_K \otimes \mathbf{d}_x, \mathbf{1}_K \otimes \mathbf{d}_y) \\ &= \log \left(\frac{\max_{i=1}^K \left(\frac{d_{y,i}}{d_{x,i}} \right)}{\min_{i=1}^K \left(\frac{d_{y,i}}{d_{x,i}} \right)} \right) = \log \left(\frac{\frac{1}{\min_{i=1}^K \left(\frac{d_{x,i}}{d_{y,i}} \right)}}{\frac{1}{\max_{i=1}^K \left(\frac{d_{x,i}}{d_{y,i}} \right)}} \right) = \log \left(\frac{\max_{i=1}^K \left(\frac{d_{x,i}}{d_{y,i}} \right)}{\min_{i=1}^K \left(\frac{d_{x,i}}{d_{y,i}} \right)} \right) = d_H(\mathbf{d}_x, \mathbf{d}_y). \end{aligned} \quad (131)$$

Thus, the lemma has been proved. \square

Then we prove the Theorem 5. Towards the p -PAM symbols in Rayleigh channel with domain $[0, +\infty)$, the channel matrix \mathbf{H} remains non-negative. Due to the difference on \mathbf{M} in DIF and RIF, we analyze them respectively.

DIF: When $N \geq K$, \mathbf{H} is a non-negative matrix with full rank in row, which means

$$[\mathbf{H}\mathbf{H}^\top]_{i,j} \geq 0, \quad i, j \in \{1, \dots, K\}. \quad (132)$$

Meanwhile, Lemma 1 reveals that $\mathbf{H}\mathbf{H}^\top$ is a PDM when $N \geq K$. Based on the properties of M matrices [42], the inverse of a positive-defined M matrix is the positive-defined non-negative matrix which is a necessary and sufficient condition. So we learn that $\mathbf{M} = (\mathbf{H}\mathbf{H}^\top)^{-1}$ is a M matrix whose elements can be represented by

$$m_{i,j} = [(\mathbf{H}\mathbf{H}^\top)^{-1}]_{i,j} = \begin{cases} \text{non-negative,} & i = j; \\ \text{non-positive,} & i \neq j. \end{cases} \quad (133)$$

RIF: In RIF, since $\frac{K}{\rho} \geq 0$ and the situation $\frac{K}{\rho} = 0$ happened only when $\rho \rightarrow +\infty$, we learn that $\frac{K}{\rho}\mathbf{I}$ is non-negative. Combining Eq. (132), it reveals that

$$\left[\frac{K}{\rho}\mathbf{I} + \mathbf{H}\mathbf{H}^\top \right]_{i,j} = \left[\frac{K}{\rho}\mathbf{I} \right]_{i,j} + [\mathbf{H}\mathbf{H}^\top]_{i,j} \geq 0, \quad (134)$$

where $i, j \in \{1, \dots, K\}$. As the same reason in DIF, we learn that $\mathbf{M} = \left(\frac{K}{\rho}\mathbf{I} + \mathbf{H}\mathbf{H}^\top \right)^{-1}$ is a M matrix whose elements can be represented by

$$m_{i,j} = \left[\left(\frac{K}{\rho}\mathbf{I} + \mathbf{H}\mathbf{H}^\top \right)^{-1} \right]_{i,j} = \begin{cases} \text{non-negative,} & i = j; \\ \text{non-positive,} & i \neq j. \end{cases} \quad (135)$$

Since $\mathbf{A}\mathbf{A}^\top$ is non-negative in Theorem 5, we have

$$\begin{aligned} [\mathbf{G}]_{i,j} &= [(\mathbf{A}\mathbf{A}^\top) \circ \mathbf{M}]_{i,j} \\ &= [\mathbf{A}\mathbf{A}^\top]_{i,j} \times m_{i,j} = \begin{cases} \text{non-negative} \times \text{non-negative,} & i = j; \\ \text{non-negative} \times \text{non-positive,} & i \neq j, \end{cases} = \begin{cases} \text{non-negative,} & i = j; \\ \text{non-positive,} & i \neq j. \end{cases} \end{aligned} \quad (136)$$

According to Lemma 1, \mathbf{G} is a PDM, and \mathbf{G}^{-1} is non-negative due to the properties of M matrix [42]. Thus, \mathbf{G}^{-1} can be regarded as a positive transformation. Based on the Perron-Frobenius theorem in direction and Hilbert metric, we have

$$\exists \gamma \in (0, 1), \quad d_H(\mathbf{G}^{-1}\mathbf{d}_x, \mathbf{G}^{-1}\mathbf{d}_y) \leq \gamma d_H(\mathbf{d}_x, \mathbf{d}_y) \quad (137)$$

for all $\mathbf{d}_x, \mathbf{d}_y \in \Omega$. Let function $g(\mathbf{d}) \triangleq \Gamma(\mathbf{G}^{-1}(\mathbf{1}_K \odot \mathbf{d}))$, in which $\Gamma(\mathbf{x})$ can be regarded as a scaling operation on \mathbf{x} . Combining Lemma 4, we have

$$\begin{aligned} & d_H(g(\mathbf{d}_x), g(\mathbf{d}_y)) \\ &= d_H(\Gamma(\mathbf{G}^{-1}(\mathbf{1}_K \odot \mathbf{d}_x)), \Gamma(\mathbf{G}^{-1}(\mathbf{1}_K \odot \mathbf{d}_y))) \\ &= d_H(\mathbf{G}^{-1}(\mathbf{1}_K \odot \mathbf{d}_x), \mathbf{G}^{-1}(\mathbf{1}_K \odot \mathbf{d}_y)) \\ &\leq \gamma d_H(\mathbf{1}_K \odot \mathbf{d}_x, \mathbf{1}_K \odot \mathbf{d}_y) = \gamma d_H(\mathbf{d}_x, \mathbf{d}_y). \end{aligned} \quad (138)$$

$d_H(g(\mathbf{d}_x), g(\mathbf{d}_y)) \leq \gamma d_H(\mathbf{d}_x, \mathbf{d}_y)$ reflects that the function $g(\mathbf{d})$ is a contraction within Ω , which means Eq. (75) will converge to a fixed direction satisfied Eq. (76). The theorem has been proved.

APPENDIX D

PROOF ON THEOREM 7

The proof of Theorem 7 consists of the derivations on DIF and RIF. We introduce them as following:

i) DIF: Since $\mathbf{E} \sim \mathcal{N}(0, \sigma_e^2 \mathbf{I})$, it can derive that $\mathbb{E}_{\mathbf{E}}(\mathbf{E}) = \mathbf{0}_K$ and $\mathbb{E}_{\mathbf{E}}[\mathbf{E}^\top \mathbf{E}] = \sigma_e^2 \mathbf{I}$. Combining Eq. (6) and the independence between \mathbf{E} and $\hat{\mathbf{H}}$, we have

$$\begin{aligned} & \mathbb{E}_{\mathbf{E}}[\|\mathbf{HP} - \mathbf{DA}\|_F^2] \\ &= \mathbb{E}_{\mathbf{E}}[\|\mathbf{F} + \mathbf{EP}\|_F^2] \\ &= \|\mathbf{F}\|_F^2 + \mathbb{E}_{\mathbf{E}}[\|\mathbf{EP}\|_F^2] + 2\text{Tr}((\mathbf{F})^\top \mathbb{E}_{\mathbf{E}}[\mathbf{E}]\mathbf{P}) \\ &= \|\mathbf{F}\|_F^2 + \text{Tr}(\mathbf{P}^\top \mathbb{E}_{\mathbf{E}}[\mathbf{E}^\top \mathbf{E}]\mathbf{P}) \\ &= \text{Tr}(\mathbf{F}^\top \mathbf{F}) + K\sigma_e^2 \text{Tr}(\mathbf{P}^\top \mathbf{P}), \end{aligned} \quad (139)$$

where $\mathbf{F} = \hat{\mathbf{H}}\mathbf{P} - \mathbf{DA}$. By assuming $g(\mathbf{P}) = \text{Tr}(\mathbf{F}^\top \mathbf{F}) + K\sigma_e^2 \text{Tr}(\mathbf{P}^\top \mathbf{P})$, we can derive the optimal precoder by

$$\begin{aligned} \frac{\partial g(\mathbf{P})}{\partial \mathbf{P}} &= \hat{\mathbf{H}}^\top (\hat{\mathbf{H}}\mathbf{P} - \mathbf{DA}) + K\sigma_e^2 \mathbf{P} = \mathbf{0}_K \\ &\Rightarrow (\hat{\mathbf{H}}^\top \hat{\mathbf{H}} + K\sigma_e^2 \mathbf{I}) \mathbf{P} = \hat{\mathbf{H}}^\top \mathbf{DA} \\ &\Rightarrow \mathbf{P} = (\hat{\mathbf{H}}^\top \hat{\mathbf{H}} + K\sigma_e^2 \mathbf{I})^{-1} \hat{\mathbf{H}}^\top \mathbf{DA}. \end{aligned} \quad (140)$$

According to the celebrated matrix inversion lemma [50], we have

$$\mathbf{P} = \hat{\mathbf{H}}^\top (\hat{\mathbf{H}}\hat{\mathbf{H}}^\top + K\sigma_e^2 \mathbf{I})^{-1} \mathbf{DA}. \quad (141)$$

Considering the power constraint, the optimal estimation-error-considered precoder in DIF is

$$\mathbf{P}_{\text{DIF}}^{\text{MMSE}} = \frac{1}{\eta} \hat{\mathbf{H}}^\top (\hat{\mathbf{H}}\hat{\mathbf{H}}^\top + K\sigma_e^2 \mathbf{I})^{-1} \mathbf{DA}. \quad (142)$$

ii) **RIF**: By assuming the regularization parameter λ for the constraint in Eq. (1), the target function in RIF is

$$\min_{\mathbf{P}} \mathbb{E}_{\mathbf{E}} [\|\mathbf{HP} - \mathbf{DA}\|_F^2] + \lambda (\text{Tr}(\mathbf{P}^\top \mathbf{P}) - \rho). \quad (143)$$

With the same process in DIF, we have

$$g(\mathbf{P}) = \text{Tr}(\mathbf{F}^\top \mathbf{F}) + (\lambda + K\sigma_e^2) \text{Tr}(\mathbf{P}^\top \mathbf{P}) - \lambda\rho. \quad (144)$$

By calculating $\frac{\partial g(\mathbf{P})}{\partial \mathbf{P}} = 0$, the optimal precoder can be derived as

$$\mathbf{P} = \hat{\mathbf{H}}^\top \left(\hat{\mathbf{H}}\hat{\mathbf{H}}^\top + (K\sigma_e^2 + \lambda)\mathbf{I} \right)^{-1} \mathbf{DA}. \quad (145)$$

Due to the uplink-downlink duality of IF precoding [22] and equal power distribution assumption [20], λ can be selected as $\lambda = \frac{K}{\rho}$, and the RIF's optimal estimation-error-considered precoder under power constraint is

$$\mathbf{P}_{\text{RIF}}^{\text{MMSE}} = \frac{1}{\eta} \hat{\mathbf{H}}^\top \left(\hat{\mathbf{H}}\hat{\mathbf{H}}^\top + \left(K\sigma_e^2 + \frac{K}{\rho} \right) \mathbf{I} \right)^{-1} \mathbf{DA}. \quad (146)$$

APPENDIX E

PROOF ON THEOREM 8

We prove Theorem 8 on DIF and RIF, which is introduced respectively as following.

i) **DIF**: According to the model $\mathbf{H} = \beta\hat{\mathbf{H}} + \boldsymbol{\Xi}$, $\boldsymbol{\Xi}|\hat{\mathbf{H}} \sim \mathcal{N}(\mathbf{0}_K, \sigma_\xi^2\mathbf{I})$, we can derive that $\mathbb{E}_{\boldsymbol{\Xi}|\hat{\mathbf{H}}}[\boldsymbol{\Xi}] = \mathbf{0}_K$ and $\mathbb{E}_{\boldsymbol{\Xi}|\hat{\mathbf{H}}}[\boldsymbol{\Xi}^\top \boldsymbol{\Xi}] = \sigma_\xi^2\mathbf{I}$. Thus, we have

$$\begin{aligned} & \mathbb{E}_{\boldsymbol{\Xi}|\hat{\mathbf{H}}} [\|\mathbf{HP} - \mathbf{DA}\|_F^2] \\ &= \mathbb{E}_{\boldsymbol{\Xi}|\hat{\mathbf{H}}} [\|\mathbf{F} + \boldsymbol{\Xi}\mathbf{P}\|_F^2] \\ &= \|\mathbf{F}\|_F^2 + \mathbb{E}_{\boldsymbol{\Xi}|\hat{\mathbf{H}}} [\|\boldsymbol{\Xi}\mathbf{P}\|_F^2] + 2\text{Tr} \left((\mathbf{F})^\top \mathbb{E}_{\boldsymbol{\Xi}|\hat{\mathbf{H}}} [\boldsymbol{\Xi}] \mathbf{P} \right) \\ &= \|\mathbf{F}\|_F^2 + \text{Tr} \left(\mathbf{P}^\top \mathbb{E}_{\boldsymbol{\Xi}|\hat{\mathbf{H}}} [\boldsymbol{\Xi}^\top \boldsymbol{\Xi}] \mathbf{P} \right) \\ &= \text{Tr}(\mathbf{F}^\top \mathbf{F}) + K\sigma_\xi^2 \text{Tr}(\mathbf{P}^\top \mathbf{P}), \end{aligned} \quad (147)$$

where $\mathbf{F} = \beta\hat{\mathbf{H}}\mathbf{P} - \mathbf{DA}$. Assume $g(\mathbf{P}) = \text{Tr}(\mathbf{F}^\top \mathbf{F}) + K\sigma_\xi^2 \text{Tr}(\mathbf{P}^\top \mathbf{P})$, the optimal precoder \mathbf{P} can be calculated by

$$\begin{aligned} \frac{\partial g(\mathbf{P})}{\partial \mathbf{P}} &= \beta\hat{\mathbf{H}}^\top (\beta\hat{\mathbf{H}}\mathbf{P} - \mathbf{DA}) + K\sigma_\xi^2 \mathbf{P} = \mathbf{0}_K \\ &\Rightarrow (\beta^2\hat{\mathbf{H}}^\top \hat{\mathbf{H}} + K\sigma_\xi^2\mathbf{I}) \mathbf{P} = \beta\hat{\mathbf{H}}^\top \mathbf{DA} \\ &\Rightarrow \mathbf{P} = (\beta^2\hat{\mathbf{H}}^\top \hat{\mathbf{H}} + K\sigma_\xi^2\mathbf{I})^{-1} \beta\hat{\mathbf{H}}^\top \mathbf{DA}. \end{aligned} \quad (148)$$

According to the matrix inversion lemma [50], we have

$$\mathbf{P} = \beta\hat{\mathbf{H}}^\top (\beta^2\hat{\mathbf{H}}\hat{\mathbf{H}}^\top + K\sigma_\xi^2\mathbf{I})^{-1} \mathbf{DA} = \hat{\mathbf{H}}^\top \left(\beta\hat{\mathbf{H}}\hat{\mathbf{H}}^\top + \frac{K\sigma_\xi^2}{\beta}\mathbf{I} \right)^{-1} \mathbf{DA}. \quad (149)$$

Substituting Eq. (99) in Eq. (149), we can derive that

$$\mathbf{P} = \hat{\mathbf{H}}^\top \left(\frac{\sigma_h^2}{\sigma_h^2 + \sigma_e^2} \hat{\mathbf{H}}\hat{\mathbf{H}}^\top + K \frac{\sigma_h^2 \sigma_e^2}{\sigma_h^2 + \sigma_e^2} \frac{\sigma_h^2 + \sigma_e^2}{\sigma_h^2} \mathbf{I} \right)^{-1} \mathbf{DA} = \hat{\mathbf{H}}^\top \left(\frac{\sigma_h^2}{\sigma_h^2 + \sigma_e^2} \hat{\mathbf{H}}\hat{\mathbf{H}}^\top + K\sigma_e^2\mathbf{I} \right)^{-1} \mathbf{DA}. \quad (150)$$

Considering the power constraint, the optimal estimation-error-considered precoder in DIF is

$$\mathbf{P}_{\text{DIF}}^{\text{ML}} = \frac{1}{\eta} \hat{\mathbf{H}}^\top \left(\frac{\sigma_h^2}{\sigma_h^2 + \sigma_e^2} \hat{\mathbf{H}} \hat{\mathbf{H}}^\top + K \sigma_e^2 \mathbf{I} \right)^{-1} \mathbf{D} \mathbf{A}. \quad (151)$$

ii) **RIF**: By assuming the regularization parameter λ for the constraint in Eq. (1), the target function in RIF is

$$\min_{\mathbf{P}} \mathbb{E}_{\Xi | \hat{\mathbf{H}}} [\|\mathbf{H} \mathbf{P} - \mathbf{D} \mathbf{A}\|_F^2] + \lambda (\text{Tr}(\mathbf{P}^\top \mathbf{P}) - \rho). \quad (152)$$

With the same process in DIF, we have

$$g(\mathbf{P}) = \text{Tr}(\mathbf{F}^\top \mathbf{F}) + (\lambda + K \sigma_e^2) \text{Tr}(\mathbf{P}^\top \mathbf{P}) - \lambda \rho. \quad (153)$$

By calculating $\frac{\partial g(\mathbf{P})}{\partial \mathbf{P}} = 0$, the optimal precoder can be derived as

$$\mathbf{P} = \hat{\mathbf{H}}^\top \left(\beta \hat{\mathbf{H}} \hat{\mathbf{H}}^\top + \frac{K \sigma_e^2 + \lambda}{\beta} \mathbf{I} \right)^{-1} \mathbf{D} \mathbf{A} = \hat{\mathbf{H}}^\top \left(\frac{\sigma_h^2}{\sigma_h^2 + \sigma_e^2} \hat{\mathbf{H}} \hat{\mathbf{H}}^\top + \left(K \sigma_e^2 + \frac{\lambda(\sigma_h^2 + \sigma_e^2)}{\sigma_h^2} \right) \mathbf{I} \right)^{-1} \mathbf{D} \mathbf{A}. \quad (154)$$

Due to the uplink-downlink duality of IF precoding [22] and equal power distribution assumption [20], λ can be selected as $\lambda = \frac{K}{\rho}$, and the RIF's optimal estimation-error-considered precoder under power constraint is

$$\mathbf{P}_{\text{RIF}}^{\text{ML}} = \frac{1}{\eta} \hat{\mathbf{H}}^\top \left(\frac{\sigma_h^2}{\sigma_h^2 + \sigma_e^2} \hat{\mathbf{H}} \hat{\mathbf{H}}^\top + \left(K \sigma_e^2 + \frac{K(\sigma_h^2 + \sigma_e^2)}{\rho \sigma_h^2} \right) \mathbf{I} \right)^{-1} \mathbf{D} \mathbf{A}. \quad (155)$$

APPENDIX F

PROOF ON THEOREM 9

According to the process in Appendix C, when Alg. 2 converges, we have learn that

$$d_H(g(\mathbf{d}_x), g(\mathbf{d}_y)) \leq \gamma d_H(\mathbf{d}_x, \mathbf{d}_y). \quad (156)$$

Thus, we have an inference chain denoted by

$$\begin{aligned} & d_H(\mathbf{d}^{(t+1)}, \mathbf{d}^{(t)}) \\ &= d_H(\Gamma(\mathbf{G}^{-1}(\mathbf{1}_K \otimes \mathbf{d}^{(t)})), \Gamma(\mathbf{G}^{-1}(\mathbf{1}_K \otimes \mathbf{d}^{(t-1)}))) \\ &= d_H(\mathbf{G}^{-1}(\mathbf{1}_K \otimes \mathbf{d}^{(t)}), \mathbf{G}^{-1}(\mathbf{1}_K \otimes \mathbf{d}^{(t-1)})) \\ &\leq \gamma d_H(\mathbf{1}_K \otimes \mathbf{d}^{(t)}, \mathbf{1}_K \otimes \mathbf{d}^{(t-1)}) \\ &= \gamma d_H(\mathbf{d}^{(t)}, \mathbf{d}^{(t-1)}) \\ &\leq \gamma^2 d_H(\mathbf{d}^{(t-1)}, \mathbf{d}^{(t-2)}) \\ &\quad \dots \\ &\leq \gamma^t d_H(\mathbf{d}^{(1)}, \mathbf{d}^{(0)}) \\ &= \gamma^t d_H(\mathbf{G}^{-1}(\mathbf{1}_K \otimes \mathbf{d}^{(0)}), \mathbf{d}^{(0)}). \end{aligned} \quad (157)$$

In Alg. 2, the algorithm ends at $d_H(\mathbf{d}^{(t+1)}, \mathbf{d}^{(t)}) \leq \epsilon$. Let $d_H(\mathbf{d}^{(t+1)}, \mathbf{d}^{(t)}) = \epsilon$, we can derive that

$$t_{\text{RA}} \log(\gamma) \geq \log \left(\frac{d_H(\mathbf{d}^{(t+1)}, \mathbf{d}^{(t)})}{d_H(\mathbf{d}^{(1)}, \mathbf{d}^{(0)})} \right) = \log \epsilon - \log \left(d_H(\mathbf{G}^{-1}(\mathbf{1}_K \otimes \mathbf{d}^{(0)}), \mathbf{d}^{(0)}) \right). \quad (158)$$

As $\gamma \in (0, 1)$, $\log(\gamma)$ is within $(-\infty, 0)$, so

$$t_{\text{RA}} \leq \frac{\log \epsilon - \log(d_H(\mathbf{G}^{-1}(\mathbf{1}_K \oslash \mathbf{d}^{(0)}), \mathbf{d}^{(0)}))}{\log(\gamma)}. \quad (159)$$

Regarding the bounds of γ , we employ the contraction ratio in Birkhoff-Hopf theorem which can be calculated by

$$\kappa(\mathbf{G}^{-1}) = \tanh\left(\frac{\Delta(\mathbf{G}^{-1})}{4}\right). \quad (160)$$

In Eq. (160), the projective diameter $\Delta(\mathbf{G}^{-1})$ can be calculated in [38] by

$$\Delta(\mathbf{G}^{-1}) = \max_{1 \leq i, j \leq K} d_H(\mathbf{G}^{-1} \mathbf{e}_i, \mathbf{G}^{-1} \mathbf{e}_j) = \log\left(\max_{i, j, p, q} \frac{g'_{p, i} g'_{q, j}}{g'_{p, j} g'_{q, i}}\right), \quad (161)$$

where $\mathbf{e}_i, i \in \{1, \dots, K\}$ represents the i -th column of \mathbf{I} and $g'_{i, j}, i, j \in \{1, \dots, K\}$ the $\{i, j\}$ element of \mathbf{G}^{-1} . Combining Eq. (159) and Eq. (161), we can obtain Eq. (110) and Eq. (111). The theorem has been proved.

REFERENCES

- [1] J. R. Hampton, *Introduction to MIMO Communications*. Cambridge University Press, 2013.
- [2] B. Hassibi and B. M. Hochwald, "How much training is needed in multiple-antenna wireless links?" *IEEE Trans. Inf. Theory*, vol. 49, no. 4, pp. 951–963, 2003.
- [3] Z. Wang, J. Zhang, H. Du, W. E. I. Sha, B. Ai, D. Niyato, and M. Debbah, "Extremely large-scale MIMO: fundamentals, challenges, solutions, and future directions," *IEEE Wirel. Commun.*, vol. 31, no. 3, pp. 117–124, 2024.
- [4] B. M. Hochwald, T. L. Marzetta, and V. Tarokh, "Multiple-antenna channel hardening and its implications for rate feedback and scheduling," *IEEE Trans. Inf. Theory*, vol. 50, no. 9, pp. 1893–1909, 2004.
- [5] N. Rajatheva, I. Atzeni, E. Björnson, A. Bourdoux, S. Buzzi, J.-B. Doré, S. Erkucuk, M. Fuentes, K. Guan, Y. Hu, X. Huang, J. Hultkonen, J. M. Jornet, M. Katz, R. Nilsson, E. Panayirci, K. Rabie, N. Rajapaksha, M. J. Salehi, H. Sameddeen, S. Shahabuddin, T. Svensson, O. Tervo, A. Tölli, Q. Wu, and W. Xu, "White paper on broadband connectivity in 6g," *6G Research Visions*, vol. 10. [Online]. Available: <https://par.nsf.gov/biblio/10223732>
- [6] M. H. M. Costa, "Writing on dirty paper," *IEEE Trans. Inf. Theory*, vol. 29, no. 3, pp. 439–441, 1983.
- [7] W. Yu and J. M. Cioffi, "Sum capacity of gaussian vector broadcast channels," *IEEE Trans. Inf. Theory*, vol. 50, no. 9, pp. 1875–1892, 2004.
- [8] L. Sun and M. R. McKay, "Tomlinson-harashima precoding for multiuser MIMO systems with quantized CSI feedback and user scheduling," *IEEE Trans. Signal Process.*, vol. 62, no. 16, pp. 4077–4090, 2014.
- [9] B. M. Hochwald, C. B. Peel, and A. L. Swindlehurst, "A vector-perturbation technique for near-capacity multiantenna multiuser communication-part II: perturbation," *IEEE Trans. Commun.*, vol. 53, no. 3, pp. 537–544, 2005.
- [10] Y. Avner, B. M. Zaidel, and S. S. (Shitz), "On vector perturbation precoding for the MIMO gaussian broadcast channel," *IEEE Trans. Inf. Theory*, vol. 61, no. 11, pp. 5999–6027, 2015.
- [11] S. G. a. Daniele Micciancio, *Complexity of Lattice Problems: A Cryptographic Perspective*, 1st ed., ser. The Springer International Series in Engineering and Computer Science No.671. Springer, 2002.
- [12] P. Q. Nguyen and B. Vallée, *The LLL algorithm*. Springer, 2010.
- [13] H. Vikalo and B. Hassibi, "On the sphere-decoding algorithm II. generalizations, second-order statistics, and applications to communications," *IEEE Trans. Signal Process.*, vol. 53, no. 8-1, pp. 2819–2834, 2005.
- [14] J. Zhang, J. Zhang, E. Björnson, and B. Ai, "Local partial zero-forcing combining for cell-free massive MIMO systems," *IEEE Trans. Commun.*, vol. 69, no. 12, pp. 8459–8473, 2021.
- [15] L. Chen, Z. Wang, Y. Du, Y. Chen, and F. R. Yu, "Generalized transceiver beamforming for DFRC with MIMO radar and MU-MIMO communication," *IEEE J. Sel. Areas Commun.*, vol. 40, no. 6, pp. 1795–1808, 2022.
- [16] Z. Wang, L. Liang, S. Lyu, Y. Xia, Y. Huang, and D. W. K. Ng, "Efficient statistical linear precoding for downlink massive MIMO systems," *IEEE Trans. Wirel. Commun.*, vol. 23, no. 10, pp. 14 805–14 818, 2024.

- [17] M. A. M. Albreem, A. H. A. Habbash, A. M. Abu-Hudrouss, and S. S. Ikki, "Overview of precoding techniques for massive MIMO," *IEEE Access*, vol. 9, pp. 60 764–60 801, 2021.
- [18] S. Stern and R. F. H. Fischer, "Advanced factorization strategies for lattice-reduction-aided preequalization," in *IEEE International Symposium on Information Theory, ISIT 2016, Barcelona, Spain, July 10-15, 2016*. IEEE, 2016, pp. 1471–1475.
- [19] S. Hong and G. Caire, "Reverse compute and forward: A low-complexity architecture for downlink distributed antenna systems," in *Proceedings of the 2012 IEEE International Symposium on Information Theory, ISIT 2012, Cambridge, MA, USA, July 1-6, 2012*. IEEE, 2012, pp. 1147–1151.
- [20] D. Silva, G. F. Pivaro, G. Fraidenraich, and B. Aazhang, "On integer-forcing precoding for the gaussian MIMO broadcast channel," *IEEE Trans. Wirel. Commun.*, vol. 16, no. 7, pp. 4476–4488, 2017.
- [21] O. Ordentlich and U. Erez, "Precoded integer-forcing universally achieves the MIMO capacity to within a constant gap," *IEEE Trans. Inf. Theory*, vol. 61, no. 1, pp. 323–340, 2015.
- [22] W. He, B. Nazer, and S. S. Shitz, "Uplink-downlink duality for integer-forcing," *IEEE Trans. Inf. Theory*, vol. 64, no. 3, pp. 1992–2011, 2018.
- [23] X. Qiu, T. Yang, and J. Thompson, "On lattice-based broadcasting for massive-user MIMO: practical algorithms and optimization," *IEEE Trans. Wirel. Commun.*, vol. 23, no. 11, pp. 16 544–16 558, 2024.
- [24] "Major advances in particle swarm optimization: Theory, analysis, and application," *Swarm Evol. Comput.*, vol. 63, p. 100868, 2021, withdrawn.
- [25] R. B. Venturilli and D. Silva, "Optimization of integer-forcing precoding for multi-user MIMO downlink," *IEEE Wirel. Commun. Lett.*, vol. 9, no. 11, pp. 1860–1864, 2020.
- [26] I. C. Trelea, "The particle swarm optimization algorithm: convergence analysis and parameter selection," *Inf. Process. Lett.*, vol. 85, no. 6, pp. 317–325, 2003.
- [27] C. Wang, E. K. S. Au, R. D. Murch, W. H. Mow, R. S. Cheng, and V. K. N. Lau, "On the performance of the MIMO zero-forcing receiver in the presence of channel estimation error," *IEEE Trans. Wirel. Commun.*, vol. 6, no. 3, pp. 805–810, 2007.
- [28] A. D. Dabbagh and D. J. Love, "Multiple antenna MMSE based downlink precoding with quantized feedback or channel mismatch," *IEEE Trans. Commun.*, vol. 56, no. 11, pp. 1859–1868, 2008.
- [29] F. Jiang, C. Li, and Z. Gong, "Accurate analytical BER performance for ZF receivers under imperfect channel in low-snr region for large receiving antennas," *IEEE Signal Process. Lett.*, vol. 25, no. 8, pp. 1246–1250, 2018.
- [30] T. Liu, "On basing search SIVP on np-hardness," in *Theory of Cryptography - 16th International Conference, TCC 2018, Panaji, India, November 11-14, 2018, Proceedings, Part I*, ser. Lecture Notes in Computer Science, A. Beimel and S. Dziembowski, Eds., vol. 11239. Springer, 2018, pp. 98–119.
- [31] A. K. Lenstra, H. W. Lenstra, and L. M. Lovász, "Factoring polynomials with rational coefficients," *Mathematische Annalen*, vol. 261, pp. 515–534, 1982.
- [32] S. Lyu and C. Ling, "Boosted KZ and LLL algorithms," *IEEE Trans. Signal Process.*, vol. 65, no. 18, pp. 4784–4796, 2017.
- [33] J. Wen, L. Li, X. Tang, and W. H. Mow, "An efficient optimal algorithm for the successive minima problem," *IEEE Trans. Commun.*, vol. 67, no. 2, pp. 1424–1436, 2019.
- [34] D. Wübben, D. Seethaler, J. Jaldén, and G. Matz, "Lattice reduction," *IEEE Signal Process. Mag.*, vol. 28, no. 3, pp. 70–91, 2011.
- [35] G. Birkhoff, "Extensions of jentzsch's theorem," *Transactions of the American Mathematical Society*, vol. 85, no. 1, pp. 219–227, 1957.
- [36] E. Kohlberg and J. W. Pratt, "The contraction mapping approach to the perron-frobenius theory: Why hilbert's metric?" *Math. Oper. Res.*, vol. 7, no. 2, pp. 198–210, 1982.
- [37] J. E. Carroll, "Birkhoff's contraction coefficient," *Linear algebra and its applications*, vol. 389, pp. 227–234, 2004.
- [38] B. Lemmens and R. Nussbaum, *Nonlinear Perron-Frobenius Theory*. Cambridge University Press, 2012, vol. 189.
- [39] E. Hopf, "An inequality for positive linear integral operators," *Journal of Mathematics and Mechanics*, vol. 12, no. 5, pp. 683–692, 1963.
- [40] R. A. Horn and C. R. Johnson, *Matrix analysis*. Cambridge university press, 2012.
- [41] J. Li and P. Q. Nguyen, "A complete analysis of the BKZ lattice reduction algorithm," *J. Cryptol.*, vol. 38, no. 1, p. 12, 2025.
- [42] A. Berman and R. J. Plemmons, *Nonnegative matrices in the mathematical sciences*. SIAM, 1994.
- [43] A. H. Sayed, "Adaptation, learning, and optimization over networks," *Found. Trends Mach. Learn.*, vol. 7, no. 4-5, pp. 311–801, 2014.
- [44] J. M. Altschuler, J. Weed, and P. Rigollet, "Near-linear time approximation algorithms for optimal transport via sinkhorn iteration," in *Advances in Neural Information Processing Systems 30: Annual Conference on Neural Information Processing Systems 2017, December*

- 4-9, 2017, Long Beach, CA, USA, I. Guyon, U. von Luxburg, S. Bengio, H. M. Wallach, R. Fergus, S. V. N. Vishwanathan, and R. Garnett, Eds., 2017, pp. 1964–1974.
- [45] T. Tao, *Topics in random matrix theory*. American Mathematical Soc., 2012, vol. 132.
- [46] C. Li, F. Jiang, C. Meng, and Z. Gong, “A new turbo equalizer conditioned on estimated channel for MIMO MMSE receiver,” *IEEE Commun. Lett.*, vol. 21, no. 4, pp. 957–960, 2017.
- [47] D. Tse and P. Viswanath, *Fundamentals of wireless communication*. Cambridge university press, 2005.
- [48] S. P. Boyd and L. Vandenberghe, *Convex optimization*. Cambridge university press, 2004.
- [49] W. Rudin, “Principles of mathematical analysis,” *3rd ed.*, 1976.
- [50] J. Zhan, B. Nazer, U. Erez, and M. Gastpar, “Integer-forcing linear receivers,” *IEEE Trans. Inf. Theory*, vol. 60, no. 12, pp. 7661–7685, 2014.